

Politecnico di Torino

**Master course in
Energy and Nuclear Engineering**

Master Thesis

Energetic Characterization of a Parabolic Solar Dish Concentrator



Supervisor:
Prof. Pietro Asinari

Research Advisor:
Matteo Morciano

Candidate:
Gianluca Ciaccio

Academic Year 2016/2017

Index

Abstract.....	4
1 Introduction	5
1.1 Introduction on solar radiation	8
1.2 Introduction on solar collectors	11
1.2.1 Flat Plate Collectors	13
1.2.2 Vacuum Tubes collectors	14
1.3 Introduction on solar water thermal systems	15
2 Concentrated Solar Power (CSP) state of the art	17
2.1 Main concentration technologies	17
2.1.1 Parabolic Trough	19
2.1.2 Solar Towers.....	21
2.1.3 Parabolic dish	23
2.2 Radiation concentration.....	24
3 Experimental Set Up and System Description.....	25
3.1 Trinum turbocaldo-parabolic dish reflector system thermal characteristics.....	26
3.2 Concentrator.....	27
3.3 Receiver	29
3.4 Hydraulic circuit.....	31
3.5 Control System.....	31
3.5.1 Hydraulic Cabinet	32
3.5.2 Electrical Cabinet.....	33
3.6 Heat exchanger	34
4 Energetic Characterization	36
4.1 Instantaneous Efficiency and Thermal Power	36
4.2 Solar radiations definitions and measurements.....	37
4.4 Experimental data analysis.....	39
4.5 Receiver modelling and check with experimental data.....	55
4.5.1 The model.....	55
4.5.2 Check with experimental data.....	57
5 Coupling of the INNOVA parabolic solar concentrator dish with a desalination unit: feasibility study.....	65

5.1	Membrane distillation.....	65
5.2	Feasibility study	67
5.2.1	Turin, Italy	67
5.2.2	Amman, Jordan	68
5.2.3	Diathermic oil	68
	Conclusions	70
	Reference List.....	72
	Acknowledgements.....	74

Abstract

Fossil fuels have been exploited at their highest rate by mankind in the last century, therefore it has been necessary, since a few decades, to increase substantially the use of clean and renewable sources of energy, in order to preserve our planet and because of the shortening of fossil fuels deposits. Whilst Europe demonstrated itself being well disposed in changing for a greater good, other countries demand their opportunity to develop thanks to fossil fuels, such as China and India, and others refuse to consider it as a problem.

Solar radiation seems to be one of the most interesting and promising sources for the future and it has undergone a big development in the past decades. The aim of this work is to study the new solar parabolic solar concentrator with double-axis sun tracking system, produced by INNOVA, for solar heating and domestic hot water production.

This work is organized as follows: chapter 1 provides brief introduction on Europe situation in terms of regulations and energy from renewable sources, and an introduction on solar radiation technologies; chapter 2 reviews concentrated solar power existing technologies and their operation; in chapter 3 the experimental setup installed in Politecnico di Torino and the acquired data are described, then in chapter 4 the performance of the solar collector are presented, in chapter 5 a brief feasibility study on the coupling of the INNOVA system with a desalination unit is described.

Chapter 1

1 Introduction

The fast consumption of fossil fuels to fulfill the request in terms of thermal energy is leading to big environmental damages and heavy deposit shortage, it is therefore necessary to go through an energetic transition, empowering and pursuing the research for alternative and renewable energy sources.

The first official meeting between nations with this purpose took place in Rio de Janeiro in 1992, and the United Nations Framework Convention on Climate Change (UNFCCC) treaty was adopted, with the aim of reducing greenhouse gas emissions, on the base of global warming. The treaty, as originally stipulated, did not set mandatory limits for the emissions to the single nations, but included the possibility that in special further acts, called "protocols", limits and obligations could be added. The most important of these acts was adopted in 1997: The Kyoto Protocol, which has become more famous than the UNFCCC itself.

The UNFCCC was opened for ratification on May 1992 and entered into force on March 1994. Its declared objective is to achieve the stabilization of atmospheric concentrations of greenhouse gases "at a level that would prevent dangerous anthropogenic (human induced) interference with the climate system." [1]. Since 1995, the parties have met annually in the "Conference of the Parties (COP)" to analyze progress in tackling the phenomenon of climate change. One of the most significant COPs of the last decade has been the COP 21, in which parties negotiated the Paris Agreement, in 2015.

Paris Agreement is a global agreement on climate change reduction, which received the consent of all the 195 participating parties, and whose aim was to limit the global warming at less than 2°C with respect to pre-industrial levels, and furthermore, to reach the no-emission of greenhouse gas from anthropic sources. This document was adopted on 12 December 2015, but the agreement would become legally binding if ratified by at least 55 countries, which together account for 55% of greenhouse gas emissions. The Paris Agreement has become effective on 4 November 2016. [2]

In June 2017, U.S. President Donald Trump announced his intention to withdraw the United States from the agreement, causing widespread condemnation all over the world. The earliest effective date of withdrawal, under the agreement, for the U.S. is November 2020, shortly before the end of President Trump's first term.

Besides Cops, on 3rd March 2010 the European Commission proposed a 10-year strategy with the aim of following a smart, sustainable, inclusive growth with greater participation and coordination at a European-level. This strategy identifies three main targets concerning environment and energy: [3]

- Reduce greenhouse gas emissions by at least 20% with respect to 1990 levels
- Achieve a 20% energy efficiency increase
- Increase the share of renewable energy in total energy consumption up to 20%.

These values can be reached only throughout the development of renewable resources, among these, solar radiation may play a fundamental role, being considered one of the most interesting and promising source since it is free and available all over the world. According to recent studies, in case of best scenario (full R&D and Policy – RDP) solar thermal could reach, with heavy financial support, a share of 6.3% out of the 20% total. According to less optimistic previsions, in business as usual conditions, the share rate would decrease to 2.4%.

As it can be seen in the following charts, Italy is a “virtuous state” having already reached in 2015 the requested share rate for 2020 (17%). Despite this, according to Eurostat data, renewable sources are developing in all Europe. Due to these positive results the European Union has set a new goal for 2030, reaching a share of renewable energy in total energy consumption of 30%.

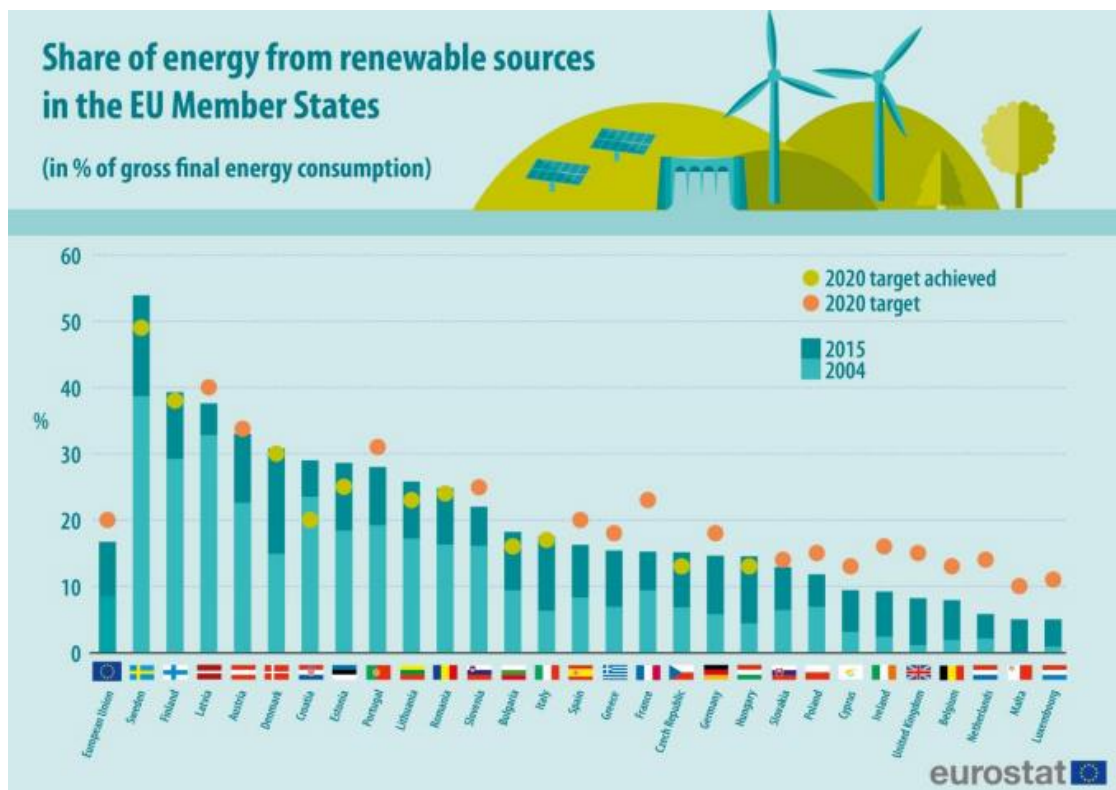


Figure 1.1: Eurostat chart describing the share of energy from renewable sources on the total production in Europe. [<http://ec.europa.eu/eurostat/web/energy/data>]

Share of energy from renewable sources
(in % of gross final energy consumption)

	2004	2012	2013	2014	2015	2020 target
EU	8.5	14.4	15.2	16.1	16.7	20
Belgium	1.9	7.2	7.5	8.0	7.9	13
Bulgaria	9.4	16.0	19.0	18.0	18.2	16
Czech Republic	6.8	12.8	13.8	15.1	15.1	13
Denmark	14.9	25.7	27.4	29.3	30.8	30
Germany	5.8	12.1	12.4	13.8	14.6	18
Estonia	18.4	25.8	25.6	26.3	28.6	25
Ireland	2.4	7.2	7.7	8.7	9.2	16
Greece	6.9	13.5	15.0	15.3	15.4	18
Spain	8.3	14.3	15.3	16.1	16.2	20
France	9.4	13.4	14.1	14.7	15.2	23
Croatia	23.5	26.8	28.0	27.9	29.0	20
Italy	6.3	15.4	16.7	17.1	17.5	17
Cyprus	3.1	6.8	8.1	8.9	9.4	13
Latvia	32.8	35.7	37.1	38.7	37.6	40
Lithuania	17.2	21.4	22.7	23.6	25.8	23
Luxembourg	0.9	3.1	3.5	4.5	5.0	11
Hungary	4.4	15.5	16.2	14.6	14.5	13
Malta	0.1	2.8	3.7	4.7	5.0	10
Netherlands	2.1	4.7	4.8	5.5	5.8	14
Austria	22.6	31.4	32.3	32.8	33.0	34
Poland	6.9	10.9	11.4	11.5	11.8	15
Portugal	19.2	24.6	25.7	27.0	28.0	31
Romania	16.3	22.8	23.9	24.8	24.8	24
Slovenia	16.1	20.8	22.4	21.5	22.0	25
Slovakia	6.4	10.4	10.1	11.7	12.9	14
Finland	29.2	34.4	36.7	38.7	39.3	38
Sweden	38.7	51.1	52.0	52.5	53.9	49
United Kingdom	1.1	4.6	5.7	7.1	8.2	15
Iceland	58.9	72.5	71.7	70.5	70.2	64
Norway	58.1	65.6	66.7	69.4	69.4	67.5
Albania	28.1	35.2	33.2	32.0	34.9	38
Montenegro	:	41.6	43.7	44.1	43.1	33
FYR of Macedonia	15.7	18.1	18.5	19.6	19.9	28
Turkey	16.2	13.1	14.0	13.7	13.6	-

: Data not available

- not applicable

The source dataset can be found [here](#).

ec.europa.eu/eurostat 

*Table 1.1: Eurostat chart describing the trend of the share of energy from renewable sources on the total production in Europe from 2004 to 2020 (target).
[<http://ec.europa.eu/eurostat/web/energy/data>]*

1.1 Introduction on solar radiation

The Sun is a sphere of intensely hot gaseous matter, considered as a black body at a temperature of 5777K and $1.5 \cdot 10^{11}$ m far from Earth, always producing energy at the inside like a continuous fusion reactor. Energy produced is then transferred to the surface and then radiated into the space according to *Planck and Stefan-Boltzmann laws* [4]:

$$E_{\lambda,b} = \frac{C_1 \lambda^{-5}}{e^{(C_2/\lambda T)} - 1} \left[\frac{W}{m^2 \cdot \mu m} \right]$$

$$E_b = \int_0^\infty E_{\lambda,b} \cdot d\lambda = \int_0^\infty \frac{C_1 \lambda^{-5}}{e^{(C_2/\lambda T)} - 1} \cdot d\lambda = \sigma T^4 \left[\frac{W}{m^2} \right]$$

Where $E_{\lambda,b}$ is monochromatic emissive power, λ is the wavelength, T is the temperature of the emitting black body, C_1 and C_2 are constants:

$$C_1 = 3.742 \cdot 10^8 \left[\frac{W \cdot \mu m^4}{m^2} \right] \quad C_2 = 1.439 \cdot 10^4 [\mu m \cdot K]$$

E_b is the total emissive power of the black body and $\sigma = 5.67 \cdot 10^{-8} \left[\frac{J}{s \cdot m^2 \cdot K^4} \right]$ is the Stefan-Boltzmann constant. [4]

For an ideal black body emitting radiations at a certain Temperature (T), there is always a wavelength (λ_{max}) which maximizes the monochromatic emissive power ($E_{\lambda,b}$). The relation between black body temperature and λ_{max} is called *Wien's law*:

$$\lambda_{max} = \frac{b}{T} \quad [\mu m]$$

Where $b = 2898 \cdot 10^3 [\mu m K]$. [4]

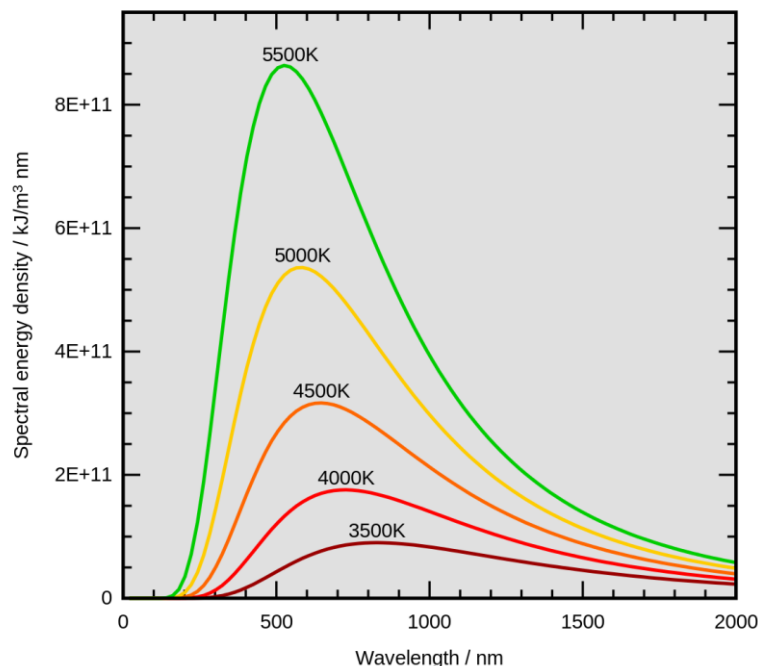


Figure 1.2: Wien's Law graphical interpretation.
<https://sites.google.com/site/rmackrellphysics/home/2010-11/s6>

It is important to state that in some solar collector applications it may be useful to know only power produced by radiations with certain wavelengths or certain range of wavelengths.

The power of solar radiation per unit area at the outer border of the Earth's atmosphere is nearly constant, and it is called solar constant, which depends on Sun's temperature, size and distance from Earth. As said before Sun's surface temperature can be considered equal to 5777 K, Sun radius r_s is about $6.965 \cdot 10^8$ m, and the mean Sun-Earth distance r_{se} amounts approximately to $1.496 \cdot 10^{11}$. On the basis of these three parameters and considering the Sun as a black body, radiation power reaching the Earth can be calculated:

First the total radiation power emitted from the sun is calculated (Stefan-Boltzmann law) [5]:

$$P_s = \sigma T^4 \cdot 4\pi r_s^2 = 3.85 \cdot 10^{26} \text{ [W]}$$

The total radiation power totally reaches any sphere around the Sun, there are no losses in the path, considering the sphere having per radius the r_{se} distance we can find the radiant energy leaving the Sun and reaching the Earth. The solar constant can be calculated dividing the radiation power P_s by the area of the considered sphere [6]:

$$G_{sc} = \frac{P_s}{4\pi r_{se}^2} = 1367 \left[\frac{W}{m^2} \right]$$

This is the power incident on a surface unit on the external border of the atmosphere in normal direction to the incident rays. In the atmosphere the solar radiation turns out to be smaller for all wavelengths, and even null for certain specific wavelengths. This reduction is due to significant phenomena which reduces solar radiation at Earth's surface:

- Atmospheric scattering:
Scattering is a continuous phenomenon due to diatomic molecules of N_2 and O_2 (Rayleigh scattering), dust and water drops, responsible of generic reduction of solar radiation.
- Atmospheric absorption:
Absorption is a discrete phenomenon which occurs only at specific spectrum bands, due to three-atoms molecules such as ozone (O_3) active in the UV bands, and water vapor (H_2O) and carbon dioxide (CO_2) in the infrared. Therefore, when reaching Earth's surface, there is almost complete absorption of UV-C, UV-B ($\lambda < 3.15 \mu m$) and IR ($\lambda > 2.5 \mu m$), taking place in the higher layers of the atmosphere [6].

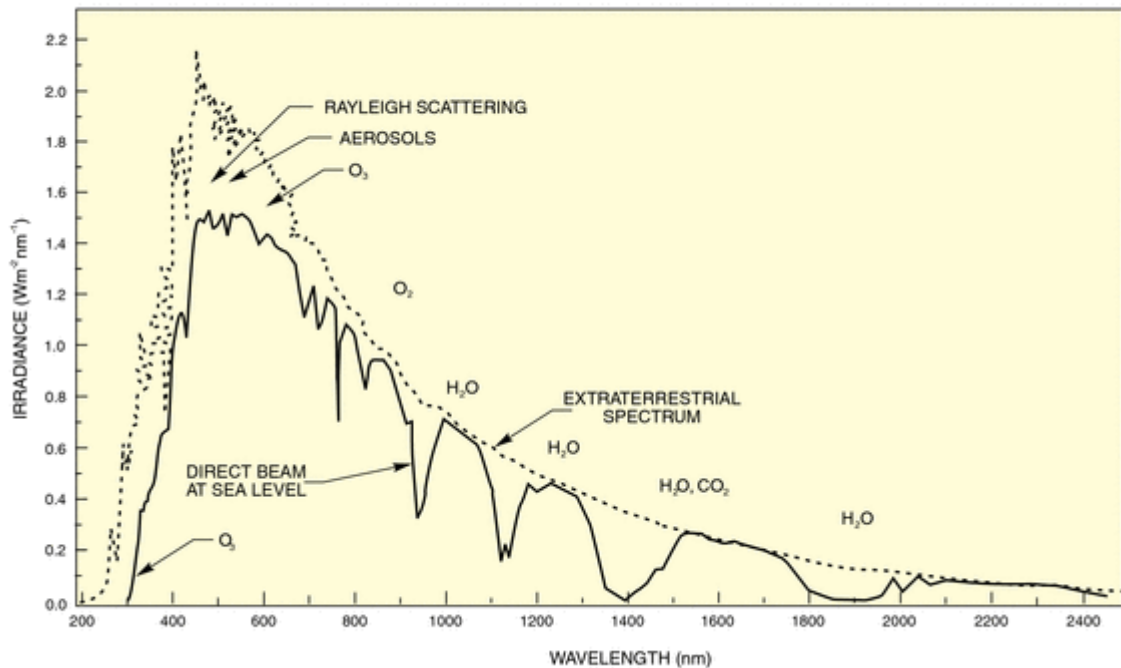


Figure 1.3: Examples of the effects of Rayleigh scattering and atmospheric absorption on the spectral distribution of beam irradiance.

[<https://www.newport.com/t/introduction-to-solar-radiation>]

The main consequence of scattering and absorption is that only the radiation of wavelength between 0.29 and 2.5 μm is significant. From an engineering point of view solar radiation reaching Earth's surface results to be split in two components: beam radiation (G_b) and diffuse radiation (G_d). The first one is the fraction of radiation reaching the surface without being scattered, the second one is the scattered fraction that undergoes scattering and is therefore diffused from atmosphere. The sum of the two is the total solar radiation (G). [5]

Furthermore, we define:

- Irradiance G [$\frac{W}{m^2}$]: rate at which the energy flux is incident on a surface per unit area of surface.
- Irradiation H [$\frac{kWh}{m^2}$]: incident energy per unit area on a surface, found by integration over a certain period (usually an hour or a day) [6].

1.2 Introduction on solar collectors

The solar collector is the heating system component dedicated to capture and transfer solar radiation to the heating fluid, therefore the aim of this device is to enhance the temperature of a certain mass flow rate of fluid, typically water or air.

A solar collector is indeed a heat exchanger, but it's quite different from traditional ones. As a matter of fact, solar collectors need a different shape, in order to let solar radiation in with as few losses as possible. The top of solar collectors is therefore covered with glasses with poor thermal insulation, therefore the case can't be considered adiabatic. This means that for each thermal gain there will be a thermal loss that can't be neglected. Solar collectors are integral receivers, because all type of radiations can produce profit [6].

There are many different types of solar collectors and they are divided into different categories according to shape and features:

- basing on radiation focusing: concentrating collectors or not concentrating collectors,
- basing on shape: evacuated tube collectors and flat plate tube collectors,
- basing on solar tracking: fixed or tracked collectors. [7]

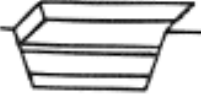
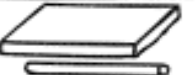
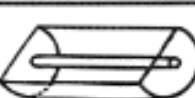
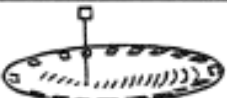
		Collector Type		Concentration Ratio, C_1 for Direct Insolation	Indicative Temperature Obtained T (K)			
		Name	Schematic Diagram					
Motion	Stationary	Non-convecting Solar Pond		Flat Absorbers	$C \leq 1$	$300 < T < 360$		
		Flat-plate Absorber			$C \leq 1$	$300 < T < 350$		
		Evacuated Envelope			$C \leq 1$	$320 < T < 460$		
	Solar Tracking	Single Axis	Compound Parabolic Reflector		Tubular Absorbers	$1 \leq C \leq 5$	$340 < T < 510$	
			Parabolic Reflector			$5 \leq C \leq 15$	$340 < T < 560$	
			Fresnel Refractor			$15 < C < 40$	$340 < T < 560$	
		Cylindrical Refractor		$10 < C < 40$		$340 < T < 540$		
		Two Axis	Parabolic Dish Reflector			Point Absorbers	$10 < C < 50$	$340 < T < 540$
			Spherical Bowl Reflector				$100 < C < 1000$	$340 < T < 1200$
	Heliostat Field			$100 < C < 300$	$340 < T < 1000$			
				$100 < C < 1500$	$400 < T < 3000$			

Table 1.2: Different types of solar collectors.
[\[http://www.thermopedia.com/content/1136\]](http://www.thermopedia.com/content/1136)

The system analyzed below in this work is a concentrated solar system that exploits as solar collector a parabolic dish reflector, the setup and the models will be discussed in following chapters. Among various energy technologies Concentrated Solar Power (CSP) is one of the most interesting and promising due to its advantages in terms of: high efficiency, low operational cost and good scale-up potential [8]. CSP

technologies exploit a system of mirrors to concentrate solar radiation on a receiver, reaching way higher temperature values than usual.

One of the major drawbacks of solar thermal is the fact that it is discontinuous because solar radiation itself is discontinuous throughout a day. Since the request is often out of phase compared to the production, some precautions must be considered, otherwise the system is not optimized [6].

1.2.1 Flat Plate Collectors

One of the main competitors of CSP systems are flat plate collectors, which are the most widespread technology in terms of thermal solar technologies. The flat plate collector is the heart of the solar energy collection system designed for operation in the low (from ambient to 60°C) to medium temperature range, usually using pressurized water as heat transfer fluid. This type of collector absorbs radiation from all wavelengths and directions, but it is important to remember that any surface is somehow selective, so its optical properties depend on wavelength and angle of incident radiation [6].

A flat plate collector usually consists of these components:

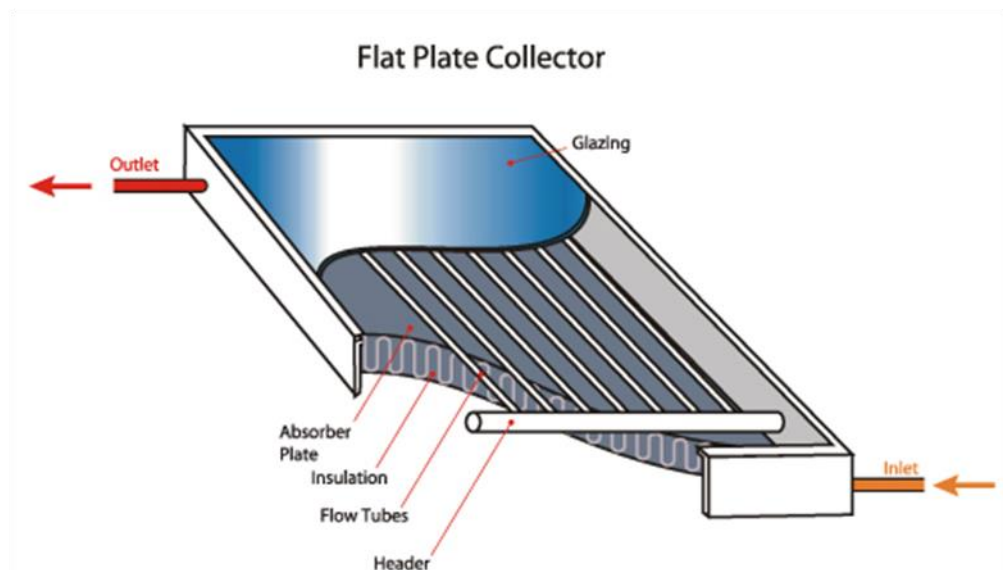


Figure 1.4: Flat-plate collector.

[<http://www.solarsense.co.za/solar-water-heating-explained.php>]

- Cover: glazing usually made of glass, it must be as transparent as possible to let the radiation in, but it should insulate the collector by absorbing infrared radiation emitted by the metal plate.
- Absorber Plate: metal plates that heats up and transfers heat to the pipes, it must be as absorbing and as low emissive as possible.

- Tubes: positioned behind the plate they transfer heat from the plate itself to the heat transfer fluid flowing from inlet to outlet. Thermal connection among plate, pipes and fluid is fundamental.
- Headers: device that receives the fluid from the circuit and handles both inlets and outlets.
- Insulation: it is needed to minimize heat losses from the back and the side of the collectors, there is no need in using a thick layer of insulant because 99% of the losses occur on the top glazing.
- Casing: protects the system from external agents [7].

Flat plate collectors are most usually mounted in a stationary position with an optimized orientation for the chosen location and the relative time of the year in which the solar system will operate. Small systems may be tilted differently from winter to summer [6].

1.2.2 Vacuum Tubes collectors

In order to increase the useful energy produced by a collector one can use selected surfaces, in order to reduce radiative losses. To fully utilize the potential of such surfaces, it is required a further reduction of the convective heat losses, which can be achieved by using more glazed covers, but it reduces incident radiation because of a major reflection. Therefore, it has been studied that this could be achieved also removing the air above the absorbing surface, this lead to vacuum tube collectors.

Vacuum tube collectors are composed of a cylindrical vacuum tube in which are allocated an absorber plate in contact with a heat pipe, which consists of a thin metal tube containing low boiling fluid which absorbs solar radiation in the lower part of the tube vaporizing and rising to the top of the pipe, where it exchanges heat with low temperature water. This makes the fluid in the pipe condense and slip down to the

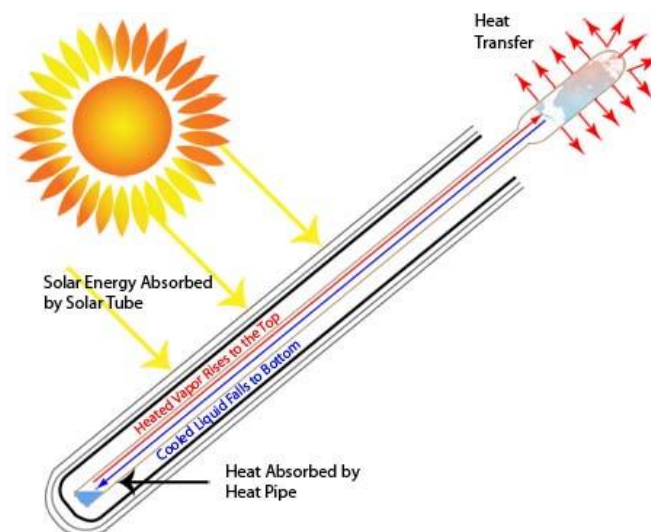


Figure 1.5: Vacuum tube collector behavior.
<http://www.solarpanelsplus.com/evacuated-tube-collectors/>

bottom of the tube, where the cycle starts again. Putting a certain number of these devices in series will produce a remarkable temperature increase in water to be heated [9].

One major disadvantage of evacuated tubes is the necessity of using a cylindrical shape, in order to hold the pressure load. It is therefore difficult to arrange the position so that the entire surface always receives the full solar flux, therefore, in commercial units the tubes are spaced apart, with reflectors behind them that reflect radiation onto the back of the tubes. As a result, these collectors are not as efficient as the flat plate at low inlet temperatures, but they are better performing at temperatures above 100°C [9].

1.3 Introduction on solar thermal water heating

There are many different possible applications for solar thermal water heating, in the analyzed system the purpose is the production of Domestic Hot Water (DHW). The demand of domestic hot water depends on people’s lifestyle, typically for Europe it is assumed around 50 l (around 0.05 m³) per person [10].

As said before one of the most important factors in the development of solar thermal technologies is the possibility of using produced energy during all day, even at night. Solar systems guarantee production in daylight hours, with a peak around 12:00, following a Gaussian pattern. In figure 1.6 it is shown the typical DHW demand, it is indeed clear that solar system usually can’t provide enough power in the high request hours, therefore a Thermal Energy Storage (TES) is mandatory. Using TES, the intermittent character of solar energy may be overcome, and systems are more economically competitive; TES are requested in over 70% of new CSP plants. [11]

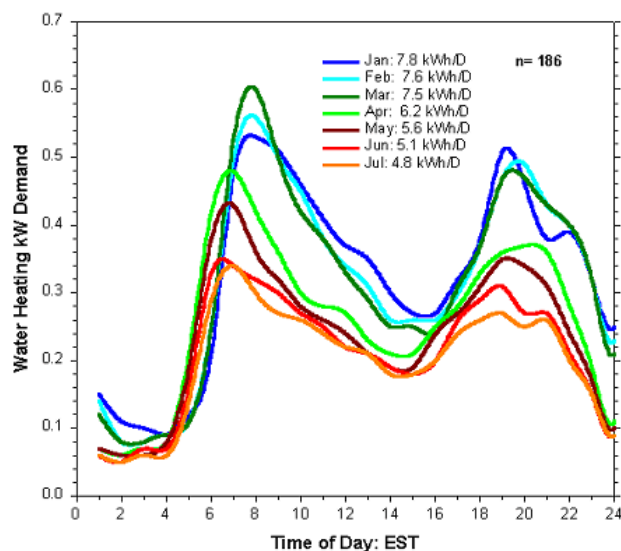


Figure 1.6: Measured DHW load profiles by month. Average of 204 residence in Central Florida. [Parker, D. S., "Research Highlights from a Large Scale Residential Monitoring Study in a Hot Climate." Proceeding of International Symposium on Highly Efficient Use of Energy and Reduction of its Environmental Impact]

There are various kinds of possible storage systems depending on which type of heat is exploited:

- Sensible heat storage, most common and used technology.
- Latent heat storage, exploiting fusion of certain selected materials (Phase Changing Materials – PCM storages), it is a new technology and there are few feedbacks.
- Thermochemical heat storages, exploiting chemical energy of products in a reversible chemical reaction, it is an experimental technology, not on the market yet [6].

The choice of storage type and media depends heavily on the nature of the process. For water heating the logical solution is a sensible heat storage based on water, because of costs and easiness of management.

The main disadvantage of solar thermal is that it is an off-grid technology, if there is an excess in production it can't be exploited, therefore systems are under dimensioned [6]. Using solar thermal only for DHW production is a reasonable but limited solution, particularly in economic terms.

Chapter 2

2 Concentrated Solar Power (CSP) state of the art

The term CSP (Concentrated Solar Power) comprises technologies used to generate gain by the concentration of direct solar beam, this profit may be in terms of electricity or thermal heat. The technology was first introduced in 1980's as result of the efforts to respond to the 1970's oil crisis, way before global warming was the main concern [12]. Since then it has been considered as an interesting technology for large scale electricity production to partly replace fossil power stations. One of the most characteristic features of this technology is that it uses direct solar radiation, and it is therefore a technology to be used in regions with excellent solar resources, and for the same reasons it needs a sun tracking system, to receive always the maximum radiation possible. One of the main advantage of CSP is indeed the fact that it can provide also base load electricity, which becomes a big advantage in economic terms [7,13,14].

2.1 Main concentration technologies

Depending on shape and purposes, different technologies have developed throughout years, the most common are:

- Line concentration systems (solar radiation is concentrated on a line):
 - Parabolic troughs:
Parabolic troughs are composed by parabolic-shape mirrors, reflecting solar radiation on an absorber pipe located in the focus of the parabola, containing the heat transfer fluid; both mirrors and absorber move.
 - Linear Fresnel:
Linear Fresnel systems are composed of a set of mirrors reflecting radiation onto one or more absorbers, unlike parabolic through, in linear Fresnel only mirrors move whilst absorbers remain stationary [13].
- Point concentration systems (solar radiation is concentrated on a point):
 - Solar towers with central receiver:
Solar tower is the most promising technology for the future, these systems are composed by a field of heliostats (almost flat mirrors) moving in order to track the sun, reflecting radiation on the top of a tower, where the receiver is placed.
 - Stirling dishes:

A Stirling dish is composed of a paraboloid reflecting surface, which diverts sun rays towards its own focus, where a Stirling engine is placed. This technology is mostly suitable for relatively low power systems [13]

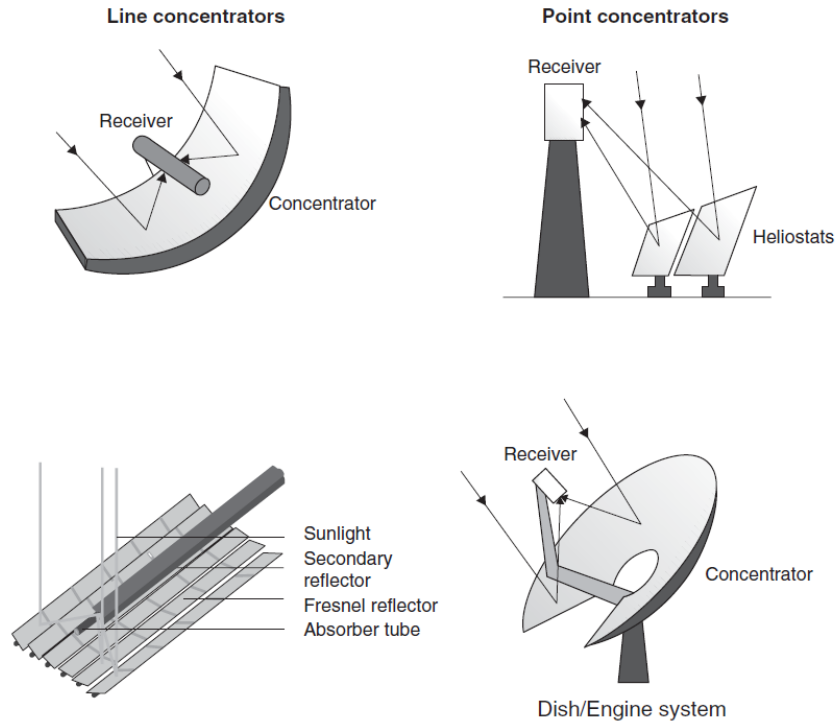


Figure 2.1: CSP technologies.
 [Robert Pitz Paal, *Future Energy - Improved, Sustainable and Clean Options for Our Planet*, 2008].

All radiation concentrating systems have in common that they need some tracking system if they shall be used continuously. As the radiation must enter the collector in a certain direction, a tracking system is required to maintain the mirrors in line with the incident direct radiation. In line concentrating systems the sun tracking engine is uniaxial, while for point concentration one it is biaxial; this means that in the first case it is cheaper but, of course less accurate [7,13,14].

- Point focusing system:

The collector zenith angle, which indicates the inclination of the concentrator in relation to the vertical is identical to the solar zenith angle, while the azimuth angle of the concentrator is equal to the solar one.

- Line focusing system:

This system requires only one tracking axis, for which are usually taken in consideration east-west alignment, which tracks sun from north to south, and north-south alignment, which tracks sun from west to east. East-west alignment needs a little collector adjustment during the day, but during early and late hours of the day performance are by far worse. North-south alignment has a much more equilibrate

daily collector performance, therefore this is the most used technology in commercial applications. [13,15]

	Capacity/ (MW _{el})	Concentration	Peak solar efficiency/ %	Annual solar efficiency/%	Thermal cycle efficiency/%	Capacity factor (solar)/ %	Land use/(m ² · (MW·h·a ⁻¹))
Trough	10–200	70–80	21 (d)	10–15 (d) 17–18 (p)	30–40 ST	24 (d) 25–70 (p)	6–8
Fresnel	10–200	25–100	20 (p)	9–11 (p)	30–40 ST	25–70 (p)	4–6
Power tower	10–150	300–1000	20 (d)	8–10 (d)	30–40 ST	25–70 (p)	8–12
Dish– Stirling	0.01–0.4	1000–3000	35 (p) 29 (d)	15–25 (p) 16–18 (d) 18–23 (p)	45–55 CC 30–40 Stirling 20–30 GT	25 (p)	8–12

¹(d): demonstrated; (p): projected; ST: steam turbine; GT: gas turbine; CC: combined cycle. Solar efficiency = net power generation/incident beam radiation. Capacity factor = solar operating hours per year/8760 hours per year.

(Source: Ref. [2])

*Table 2.1: Performance of various CSP technologies
[Robert Pitz Paal, Future Energy - Improved, Sustainable and Clean Options for Our Planet, 2008.]*

The advantages of CSP technology can be summarized as follows:

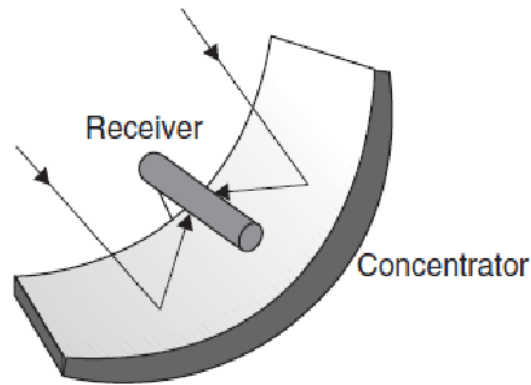
- Working temperatures up to 1000-1500 °C, depending on the heat transfer fluid used;
- Constant performance throughout the day;
- Lower dissipation due to a lower dispersing surface.

These features allow the use of concentration devices both on a domestic scale, for the supply of domestic hot water or for integration to the air conditioning system, and on the industrial one, for processes such as desalination or solar cooling [16].

2.1.1 Parabolic Trough

Parabolic through systems concentrate direct solar irradiance onto a tubular receiver placed in the focus of the parabolic through collectors. Large collector fields supply the thermal energy, which is then transferred to the heat transfer fluid. Parabolic trough is by far the dominating and most used among CSP technologies, providing around 90% of the capacity of concentrating solar power plant technologies in operation [13].

A parabolic trough power plant is usually composed by:



Parabolic Trough

Figure 2.2: Parabolic trough components.

[Robert Pitz Paal, *Future Energy - Improved, Sustainable and Clean Options for Our Planet*, 2008].

- Parabolic trough collectors: usually made of silver coated glass mirrors with a multilayered structure, it is necessary for them to be durable. Their geometry is parabolic and is described by: trough length, focal length, aperture width and rim angle. One of the most important aspect of the collector is the sun tracking system, which need information about the Sun position, calculated with algorithms or measured by sensors, to tilt the collectors to receive the maximum radiation in every moment. The totality of collectors and their arrangement on the power plant ground is called solar field.
- Receiver: since the reflected radiation must hit the absorber surface, the receiver must respect some constraints. The radiation must be converted as much as possible into heat and therefore thermal and optical losses must be minimized, special coatings and insulations are installed to achieve this. Besides the glass in tubes also all metallic parts represent an issue because of heating. The rise in temperature may cause tension problems and therefore the thermal expansion coefficient of the glass near the compensator and compensator itself must coincide. The efficiency in the receiver is dependent on both optical and thermal losses, even though the first account only for the 10% of the total.
- Heat transfer fluid: the HTF has the task of accumulating thermal energy and transporting it to the power block. Two types of HTF can be used: first, a special fluid is exploited, from which the heat is transferred to another working fluid and then stored; or second, the same fluid that flows in the absorber tubes of the parabolic through transports heat directly to the storage. First configuration is an indirect system, while the second is called direct system. [13,14,15]

Parabolic trough technology may be coupled with a thermal storage in order to store energy to cover peaks of request.

2.1.2 Solar Towers

A solar tower power plant consists of many sun-tracking mirrors which focus highly concentrated solar irradiation onto an absorber, the receiver, located on the top of the tower. The type of focusing is “point focusing”.

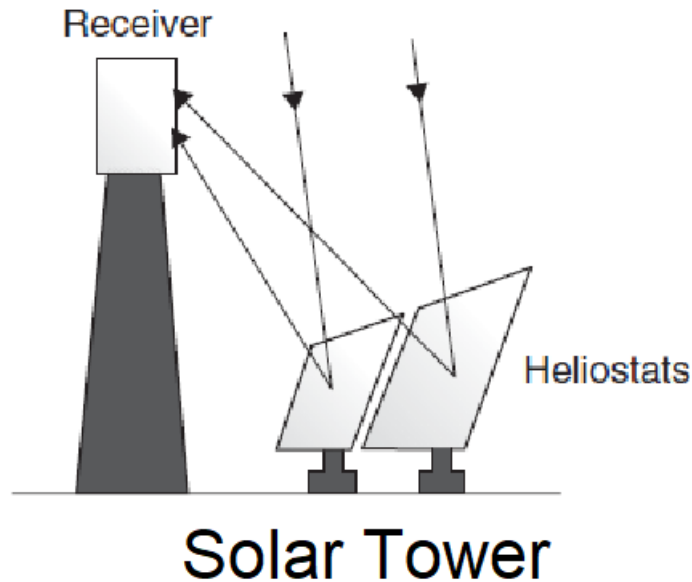


*Figure 2.3: Solar tower with central receiver system.
[Robert Pitz Paal, Future Energy - Improved, Sustainable and Clean
Options for Our Planet, 2008].*

The two most important components of a solar tower system are:

- Solar Field:

In this application the solar field is made of heliostats, which are mirrors equipped with two axes tracking system in order to track the sun's path. The heliostat field provides thermal energy for the receiver placed on the tower and therefore they must follow the sun's position over the whole day. The heliostat field makes up roughly 50% of the total investment cost [13,14,16], it is therefore fundamental to try and reduce the heliostat cost to improve the economic viability of the system.

Different types of heliostat mirrors exist, different according to size, shape, design, material and tracking system; each heliostat has its own properties in terms of cost, complexity of control and performances. Usually these mirrors are made by combination of two or more materials to improve reflecting properties.

Size is very important, reflective areas of heliostats vary from 1 m² to 150 m², the advantage of having larger sized heliostats is that since fewer heliostats are installed the maintenance costs are lower; however, the drawbacks are a more difficult installation and maintenance [13]. Lately, the trend is to develop both very large and very small mirrors.

The field design is a key topic, it was determined that it is generally best to arrange the heliostats in a radial stagger pattern, as shown in figure 2.4, configuration that minimizes land usage and ensuring better productivity. The spacing between heliostats increases along with the distance from the tower, in order to minimize the possibility of a heliostat shadowing other heliostats. Heliostat field design may also vary depending on the location [15].

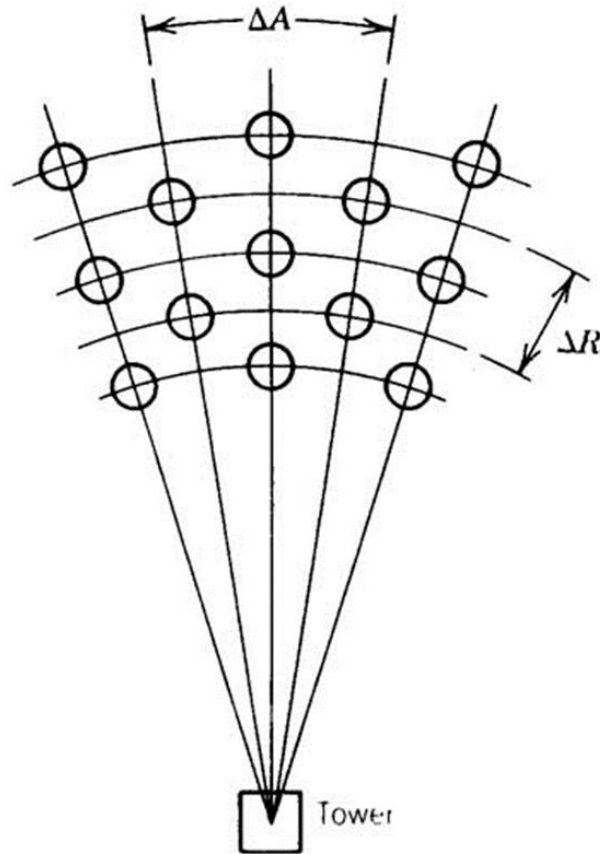


Figure 2.4: Representation of radial staggered disposition of heliostats in a solar field.

[<http://www.powerfromthesun.net/Book/chapter10/chapter10.html>]

- Receiver

As seen before the receiver's purpose is to absorb concentrated radiation and transfer it to the heat transfer fluid. There are many kinds of receiver fitting the solar tower system, two main configurations may be distinguished: first, the solar radiation hits the absorber on the tower, behind which there are pipes transporting the heat transfer fluid, that heats up; second, solar radiation enters a cavity on the top on the solar tower and hits a mirror which reflects once again the radiation onto the ground where the receiver is installed. [15]

2.1.3 Parabolic dish

Parabolic dishes, also known as PDR (Parabolic Dish Reflector), are solar collectors composed of a parabolic reflector, which conveys solar radiation on its focus, onto an absorber. Solar radiation is then converted in thermal energy exploiting the thermal fluid in the absorber, which reaches temperatures around 1500°C [13].

In order to guarantee correct reflection, the geometry of the system must be designed to convey the rays, whichever the point of incidence of these with the surface is, in the direction of the focus. A movement system with two rotation axes and a solar tracking software allow the structure to track with minimal margin of error the trajectory of the Sun throughout the day [13,14,15].

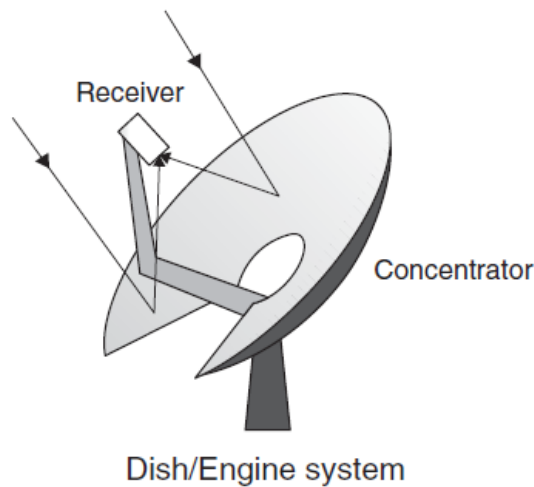


Figure 2.5: Structure of a parabolic dish reflector (PDR)
[Robert Pitz Paal, Future Energy - Improved, Sustainable and Clean Options for Our Planet, 2008].

The advantages of PDR devices are the following:

- Most efficient conversion technology, as always oriented towards the Sun;
- Concentration ratios between 600 and 2000, which allow to obtain very high operating temperatures and high conversion efficiencies.
- The modularity of the systems allows both independent uses for single units and composed structures.
- Excellent absorption efficiency and energy conversion to the fluid.

Losses due to thermal dissipation are generally very low, but they might become relevant and very damaging in case of imperfections in the parabolic shape of the reflector, which causes errors in the aiming precision. For this reason, the device requires periodic checks and, in case of damage, a prompt maintenance. Usually there are sensors for detecting the temperature in the absorber which, in the event of a malfunction, report the fault to the user, ensuring the protection of the system. [13,14,16]

2.2 Radiation concentration

Radiation concentration is an interesting technology that enhances the power extractable from solar radiation. Paraboloids concentrate radiation on a focal point, while parabolic trough on a focal line.

The concentration ratio C is defined as the ratio between radiant flux after the concentration and before the concentration; in many cases it may be approximated by the ratio of the aperture area of the optical system to the area of the image of the radiation source at the point where the area of this image is minimal [6]:

$$C = \frac{\textit{Aperture Area}}{\textit{Area of radiation source image}}$$

Since we are considering systems that concentrate solar radiation incident on the aperture area onto an absorber, and supposing that the absorber surface covers just the sun image:

$$C = \frac{\textit{Aperture Area}}{\textit{Absorber Area}}$$

Even with a theoretically perfect mirror it is impossible to achieve an infinite concentration ratio, because solar radiation does not arrive in exactly parallel rays, and, therefore, the sun's image is not concentrated in the focal point but occupies a certain area around it. It can be demonstrated that, theoretically speaking, the maximum value of the concentration ratio is: $C_{\max} = 46200$ for an ideal three-dimensional concentrating system, concentrating radiation in one spot, while for a two-dimensional system concentrating onto a line it is $C_{\max} = 215$. These values are theoretical, nowadays the maximum achievable ratios are 4000 for point focusing systems and 80 for line focusing systems. [6,17]

Chapter 3

3 Experimental Set Up and System Description.

It is now described the solar energy collector system provided by INNOVA, a parabolic solar dish reflector with two-axis tracking. The complete system scheme is shown in figure.

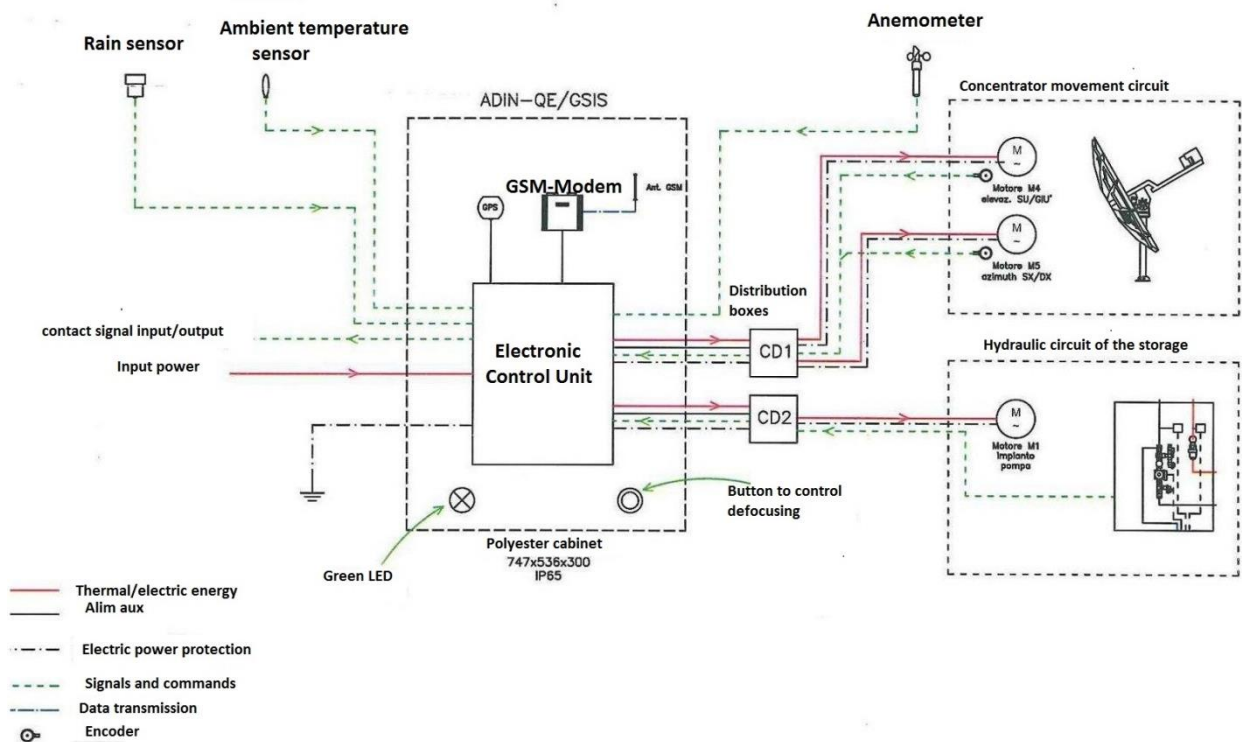


Figure 3.1: System connection scheme
[TRINUM, Technical Manual for Installation and Use, 2014]

3.1 Thermal characteristics of the turbocaldo-parabolic dish reflector system

The technical features of the Turbocaldo device have been evaluated by the Innova company in standard operating conditions and in correspondence with an installation site subject to direct irradiation throughout all day, in order to obtain the maximum working parameters.

The functional data are provided in relation to operating conditions with a clear sky and incident radiation with an intensity of $1000 \frac{W}{m^2}$. In this state, the system may produce thermal power peaks of 7.4 kW and of flow rates between $7 \frac{l}{min}$ and $19 \frac{l}{min}$ [18]. The conversion efficiency has a stable trend with the temperature difference between the collector and the external environment and remains higher throughout the working range with respect to the relative stationary conversion devices. [19]

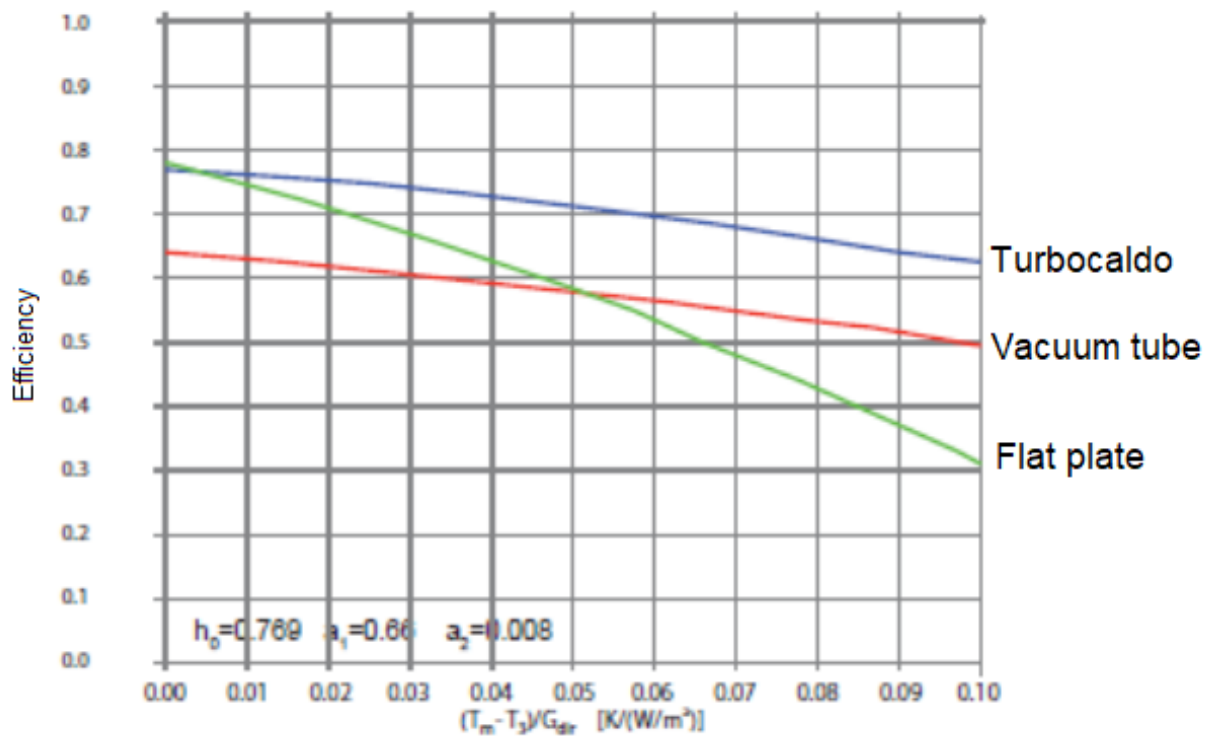


Figure 3.2: Efficiency of the Turbocaldo system with respect to the main stationary systems. [TRINUM, Technical Manual for Installation and Use, 2014]

The average optical efficiency over the entire spectrum is around 89%, kept roughly constant for all wavelengths due to the multilaminar nature of the reflector segments. [18]

3.2 Concentrator

The structure of the system is completely made of galvanized steel while the concentrator itself it is made of multilaminar reflective aluminum mirrors. The concentrator has a 9.58 m^2 effective area, collecting solar radiation and reflecting it into a metallic receiver placed in the focal point of the parabolic dish, this point is 2.26 m distant from the dish itself. An 89% optical efficiency must be considered to take into account dirt, dust and other agents, which increase optical losses.

The system has two possible configurations: working and safe conditions. In the first case the system is producing thermal power and operating normally. In the second condition the system is turned off, it is important to state that if the working conditions exceed the limits, the system will automatically go into safe position; this is possible thanks to sensors which can detect wind, rain and external agents as well as temperature, pressure or mass flow rate unjustified variations. In working conditions, the system may be set onto *Automatic*, so that it keeps tracking the sun and moving without any other support. Once the system is installed and when it is updated, the alignment with the sun must be set, it is advisable to do this in the most productive hours of the day. [18]

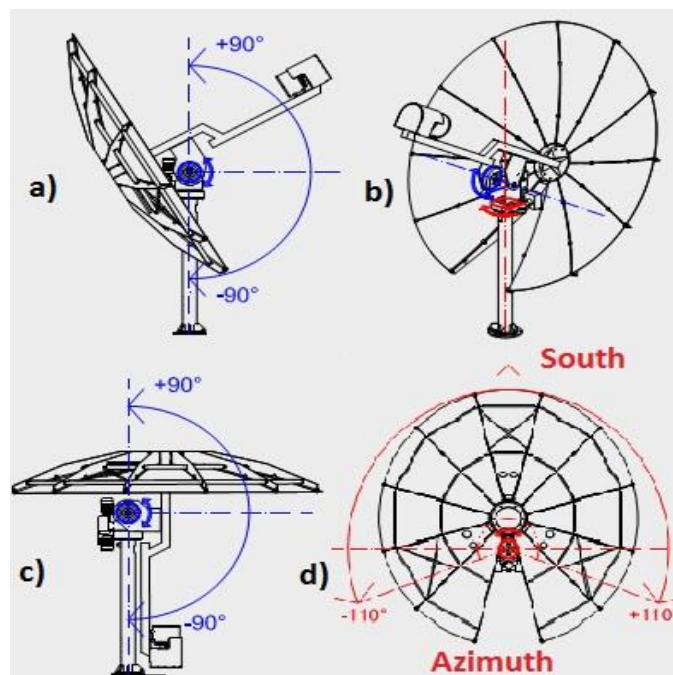


Figure 3.3: Working position: a) side view b) axonometric view. Safe position: c) side view d) plan view [TRINUM, Technical Manual for Installation and Use, 2014]

In order to utilize maximum possible solar radiation, knowledge of sun's path through the sky is necessary for proper orientation of collectors. To understand the functioning of the sun tracking system its important the definition of two solar angles:

- Elevation angle (α): is the angle between Earth-Sun line and horizon plane
- Azimuth angle (γ_z): angular displacement from the South of the projection of a Sun ray on the horizon plane (positive toward West)

The system starts tracking the sun in the morning when elevation is around 10° and turns off at sunset when elevation is around 10° . These settings may be changed depending on the solar incident radiation that hits the collector. The tracking system is independent and needs no support, the instantaneous orientation is monitored by an encoder, which sends data to the Control Unit regarding theoretical and actual elevation and azimuth, if an error is computed then the structure is shifted in order to compensate by means of two motors installed on the structure. Therefore, the percentage error between the actual and the solar trajectory is minimum.

In the following graphs it is shown a comparison between solar trajectory and the trajectory followed by the encoder, in terms of elevation and azimuth angles.

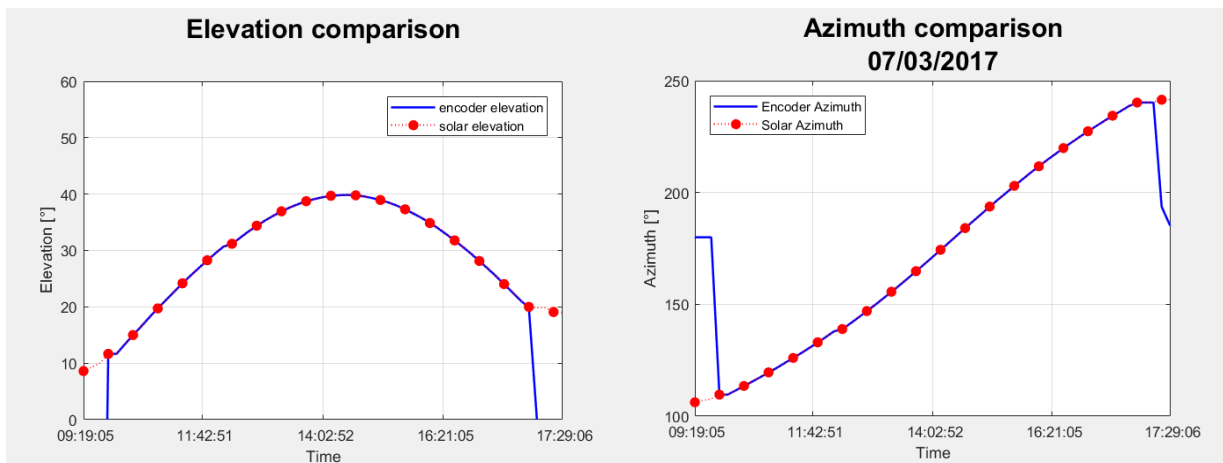


Figure 3.4: Elevation and azimuth angle comparison in March 7, 2017

These graphs show the high reliability of the sun tracking system, indeed the encoder line overlaps the solar one during functioning; as previously said, when elevation angle is low the sun tracking stops and the system shuts down, this explains the huge mismatch between the two curves out of the functioning period. [20]

3.3 Receiver

The Receiver is the element that performs the absorption function, it acts as a heat exchanger with the working fluid flowing at its inlet. It is a stainless-steel cylinder having a base circumference with a diameter of 0.33 m and height of 0.52 m. The circular opening facing the reflector, in which the solar radiation is conveyed, has a 0.2 m diameter, which corresponds to an area of 314 cm². The ratio between this surface and parabolic collector one provides the geometric concentration coefficient of the device, which in our case is $C = \frac{\text{Aperture Area}}{\text{Absorber Area}} = 305$.

The heat transfer fluid flows inside the receiver in a steel cavity, placed in direct contact with the internal cavity of the absorber. This is coated with black paint in order to increase the absorption coefficient and limit the reflection coefficient. To reduce the thermal dispersions towards the environment between the pipe and the external surface of the absorber, there is a layer of insulating material, rock wool, with a thickness of 4 cm.

The described configuration aims to guarantee the maximum net absorption of the radiation. Moreover, since the maximum working temperatures are concentrated on a closed and small area, the thermal dissipations are further limited. The receiver is still the major heat losing component in the system, therefore it is the component that most affects the performance of the system. The receiver is shown in figure 3.5. A further analysis on this component will be carried out in chapter 4. [18]



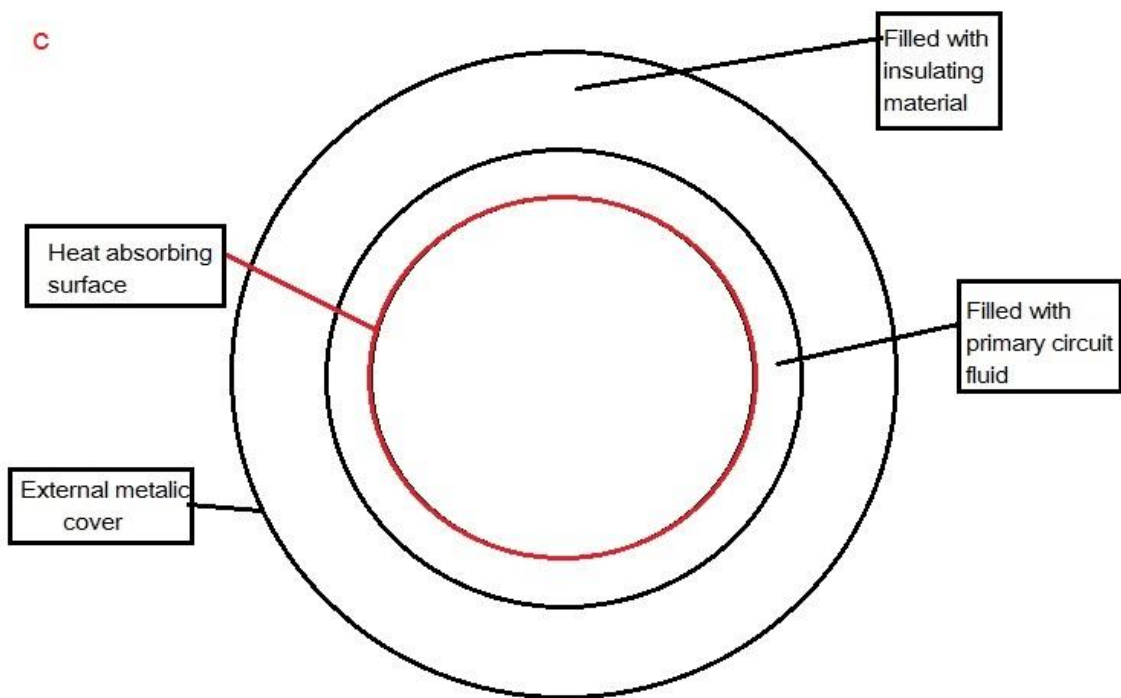


Figure 3.5: Receiver cross section, a) front view, b) backward view, c) general description



Figure 3.6: External view of both installed collector and receiver.

3.4 Hydraulic circuit

The installed system couples the parabolic dish collector and the receiver to two storage tanks with volume 1000 liters for domestic hot water production and storage. The primary circuit is defined from concentrator to heat exchanger, a water-glycol mixture (60-40) is used as working fluid and all the pipes are insulated to minimize heat losses. The secondary circuit is defined from the heat exchanger to hot water storage tanks. Both primary and secondary circuit have sensors installed in order to control parameters such as temperature, mass flow rate, pressure; these sensors send data to the Control Unit which constantly checks the correct functioning of the system. Detailed connection of hydraulic circuit is shown in figure 3.7.

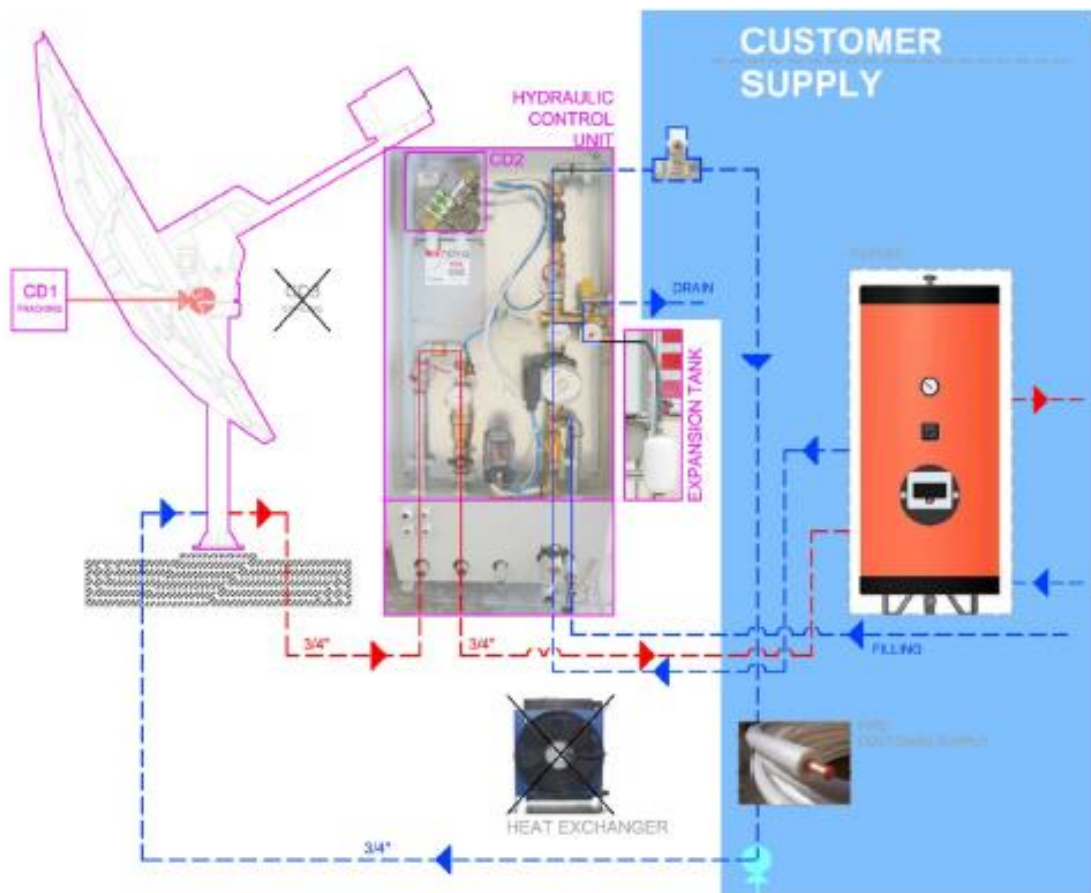


Figure 3.7: Primary loop of the hydraulic circuit.
[TRINUM, Technical Manual for Installation and Use, 2014]

3.5 Control System

The control system allows online monitoring of process parameters and networks. The involved elements are:

- Hydraulic Cabinet: evaluates the measurement of mass flow rate, temperature, pressure and produced thermal power of the primary circuit.

- Electrical Cabinet: connected to the concentrator and to the Hydraulic Cabinet through the junction boxes, it displays the data regarding the solar path, the orientation of the collector, the latitude, the number of reference satellites, the values of the Hydraulic Cabinet and the parameters referred to the secondary circuit. Throughout the display it is also possible to manage the Turbocaldo operating modes manually if necessary. [18]

3.5.1 Hydraulic Cabinet

The hydraulic cabinet contains the systems for measuring network data, throughout components such as turbine type flow meters, temperature probes, valves and circulation pumps to keep the mass flow rate between 7 and 19 $\frac{l}{min}$. The hydraulic cabinet is also connected to the electrical cabinet with a junction box. All parameters are sent to the central control unit, which provides useful information, such as the power transferred from the receiver to the working fluid.

The structure of the hydraulic cabinet is shown in figure 3.8.



Figure 3.8: Hydraulic Cabinet.
[TRINUM, Technical Manual for Installation and Use, 2014]

3.5.2 Electrical Cabinet

The Electrical Panel is the structure that contains all the electronic devices that allow the monitoring of system performance. These receive the values coming from the junction boxes installed near the concentrator and the Hydraulic Panel, the encoder and other sensors installed throughout the system and transforms them into a physical signal in the Control Unit. The main components of the electrical cabinet are shown in figure 3.9.

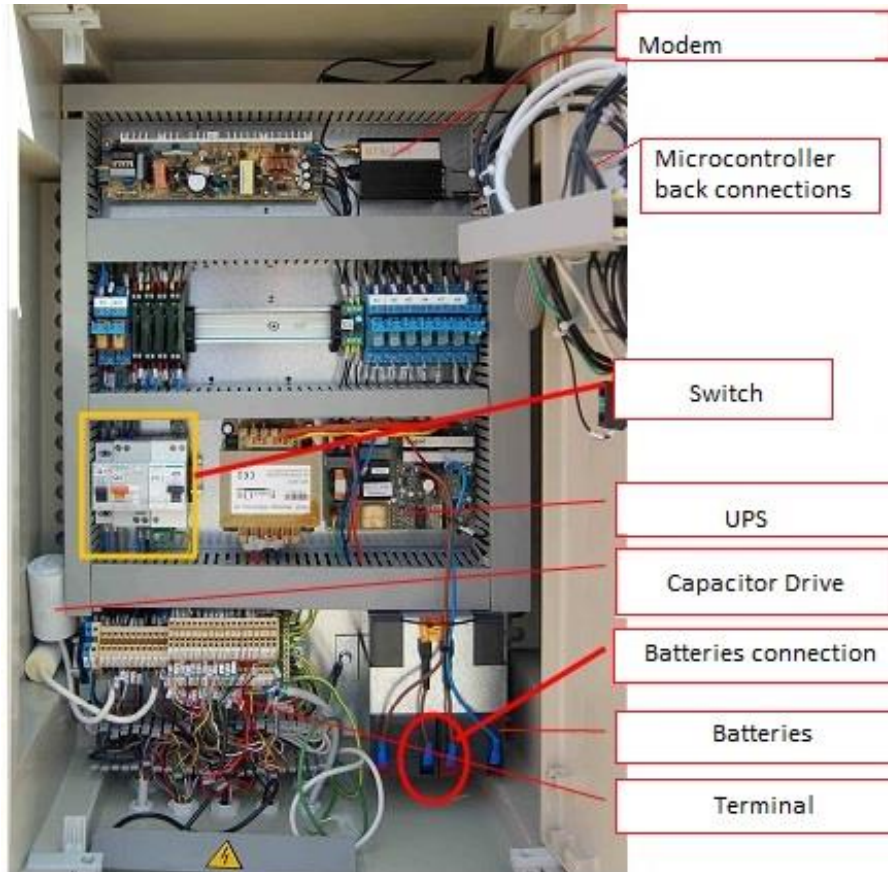


Figure 3.9: Electrical cabinet of the system with main components.
[TRINUM, Technical Manual for Installation and Use,2014]

The electrical cabinet contains a microcontroller, which performs the electronic control of the system, it is located inside the electrical cabinet. The parameters can be seen on the display, and all operations take place by means of the display, using the buttons located on the device, as shown in figure 3.10.

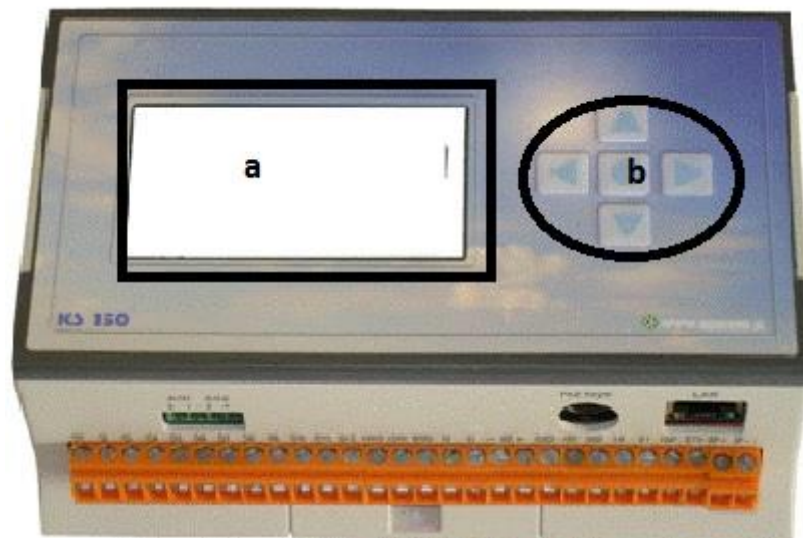


Figure 3.10: Control display a) display b) navigation buttons.
 [TRINUM, Technical Manual for Installation and Use,2014]

The following system data are displayed by the microcontroller:

Ambient Temperature [°C]	Boiler Temp [°C]
Coolant Inlet Temperature [°C]	Thermal Power [W]
Coolant Outlet Temperature [°C]	Wind Speed [km/h]
Coolant Flow Rate [l/min]	

Table 3.1: Variables received by the control unit
 [TRINUM, Technical Manual for Installation and Use,2014]

3.6 Heat exchanger

The heat exchanger is designed to transfer heat between low and medium pressure fluids, in this system it is a gasketed plate heat exchanger, whose characteristics are provided in the table 3.2. [18]

UniGasket gasketed plate
heat exchanger:

PGT14 ES32/10/6R-13IK

Fluid	:	Acqua	Acqua
Inlet Temperature	°C :	110	95
Outlet Temperature	°C :	100	105
Mass Flow Rate	kg/s :	0,19	0,19

Maximum Power Potential	kW :	8	
Total Heat Exchange Area	m ² :	0,45	
LMTD	°C :	5	
Global Heat Transfer Coefficient	W/m ² , °C :	3548	
Oversizing	% :	29	
Calculated Loss of Load	kPa :	1,4	1,4
Number of Ducts	:	1*6	1*6
Number of Plates	:		13

Construction Data:

Plate Material	:	AISI 316L	
Plate Thickness	mm :	0,6	
Gasket Material	:	EPDM UniLock	
Frame Material	:	acc.carbonio	
Bars Material	:	zincato	
Connection Material	:	AISI 304	AISI 304
Connection Diameter	in/in :	1"1/4	1"1/4
Connection Standard	:	Filettato maschio	Filettato maschio
Connection Position	entrata/uscita :	F1/F4	F3/F2
Maximum Operating Pressure	bar :		10
Test Pressure	bar :		14,8
Maximum Operating Temperature	°C :		140
Empty Weight	kg :		30
Design Code	:	PED 97/23/CE – esente art.3.3	

Table 3.2: Heat exchanger data sheet.

Chapter 4

4 Energetic Characterization

The energetic characterization of the system consists in the analysis of the parameters of efficiency and thermal power related to the treated concentration device. The data were collected in the period between February 2017 and February 2018 in order to evaluate the trend of the values both during the single day and throughout the entire month, furthermore the difference between seasons could be investigated. Finally, measurements related to specific days were evaluated, for which the weather conditions were found as similar as possible to those of clear sky.

4.1 Instantaneous Efficiency and Thermal Power

The conversion efficiency is calculated as the ratio between the power absorbed by the circulating fluid in the primary circuit, \dot{Q}_a , and the product between the direct normal irradiance, DNI, and the available surface of the solar reflector, A_r , equal to 9.58 m² [17]:

$$\eta = \frac{\dot{Q}_a}{DNI \cdot A_r} = \frac{\dot{m}c_p(T_{out} - T_{in})}{DNI \cdot A_r}$$

where:

- \dot{m} is the mass flow rate in the primary circuit in kg/s;
- c_p is the thermal capacity of the water and glycol mixture (60-40) at the operating temperature, which, in our hypothetical calculation, is constant and equal to 3,394 $\frac{kJ}{kg K}$;
- T_{out} the temperature measured at the outlet of the receiver;
- T_{in} the temperature measured at the inlet of the receiver.

4.2 Solar radiations definitions and measurements

Several radiation parameters are needed for the performance evaluation of the solar collector: total radiation, diffuse radiation and beam radiation. It is therefore necessary to define radiation components and the instrumentation to measure in tests:

- Beam radiation or direct radiation - is the solar radiation received from the sun without being scattered by the atmosphere. The concentrating collectors can utilize only this component of the radiation. The device to measure this radiation is the pyrheliometer, which measures beam radiation at normal incidence.
- Diffuse radiance - is the solar radiation received from the sun after its direction has been changed by scattering by the atmosphere. It is possible to measure diffuse radiation using the pyranometer, where the sensing element is shaded from the beam radiation.
- Total (Global) solar radiation - is the sum of beam and diffuse solar radiation on a surface, as discussed before, it is measured by means of pyranometer.
- Irradiance, $G \left[\frac{W}{m^2} \right]$ - is the rate at which radiant energy (energy flux) is incident on a surface per unit area of surface.
- Irradiation $H \left[\frac{kWh}{m^2} \right]$ - is the incident energy per unit area on a surface, found by integration of irradiance over a specified period. [20]

As previously remarked, concentrating technologies can exploit only the direct component of the global radiation, which cannot be evaluated by the instrumentation at our disposal, as the solarimeter allows the detection of only diffused radiation. Therefore, the PVG IS system (Photovoltaic Geographical Information System) was used for the analysis. It is available on the page of the European Commission Institute for Energy and Transport (IET), which makes it possible to derive all the components according to the geographical position of reference. of global radiation under real conditions and clear skies, providing daily and monthly averages. The data obtained do not take into account any conditions of overcast skies and cloudiness, therefore the study was carried out in correspondence with days with a clear sky. The following graphs show the average daily trend of direct radiation, in both condition of clear sky and real sky, on the considered dates:

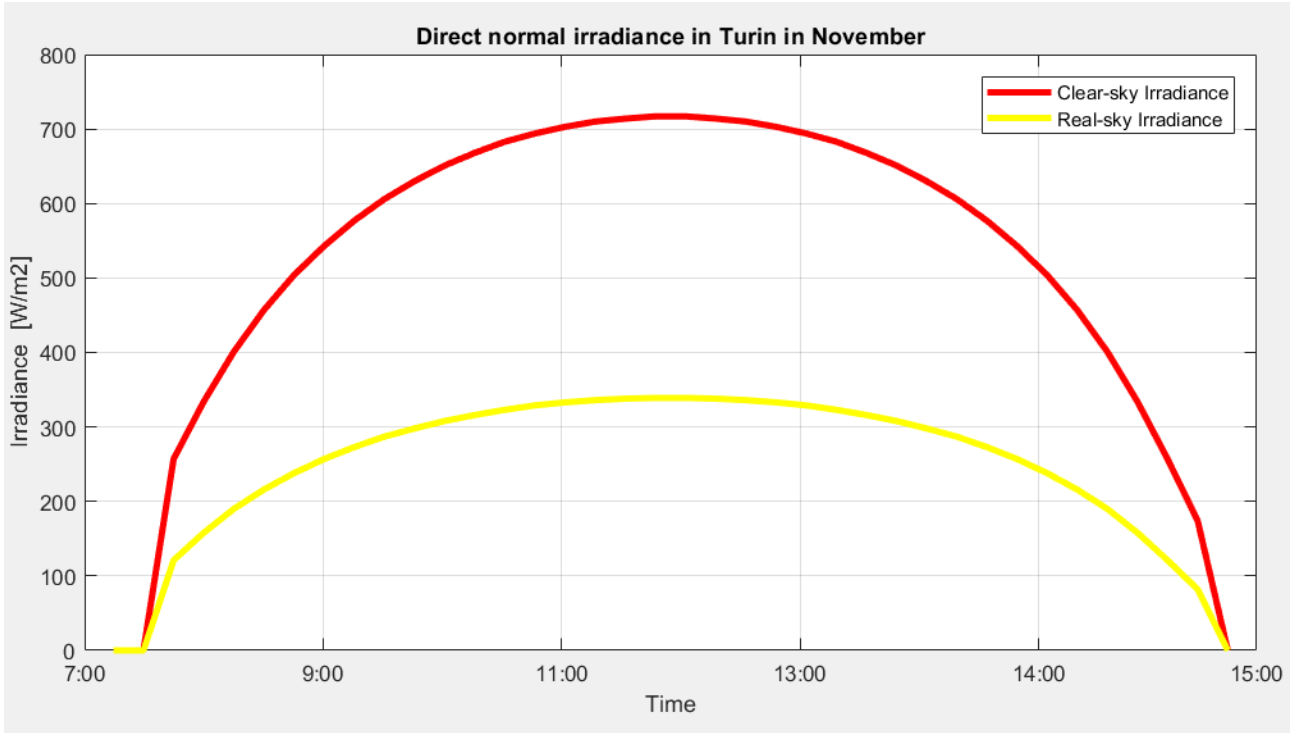


Figure 4.1: Direct normal irradiance in November from PV GIS
[\[http://re.jrc.ec.europa.eu/pvgis\]](http://re.jrc.ec.europa.eu/pvgis)

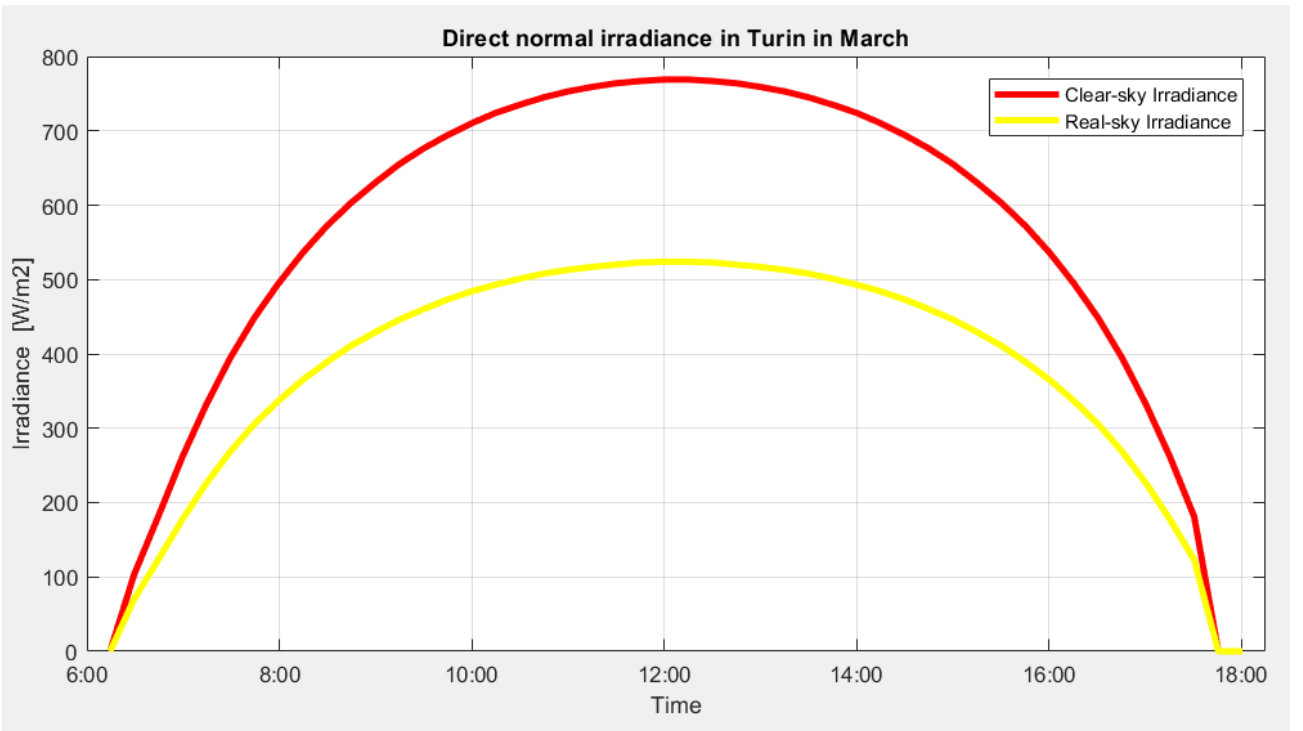


Figure 4.2: Direct normal irradiance in March from PV GIS
[\[http://re.jrc.ec.europa.eu/pvgis\]](http://re.jrc.ec.europa.eu/pvgis)

4.4 Experimental data analysis

Throughout the Control Unit of the Electrical Panel it is possible to obtain data referring to the flow rate, inlet and outlet temperatures, the temperature in the tank, the instantaneous thermal power. These data are evaluated and stored with a 10 minutes interval by electronically computed sensors. Therefore, it is possible to pursue an experimental data analysis.

This analysis was conducted throughout several months among 2017 and 2018, in order to have an overview of the difference of the parameters across the whole year. The following graphs show the trend of thermal power produced by the system and the average temperature difference between inlet and outlet throughout March 2017.

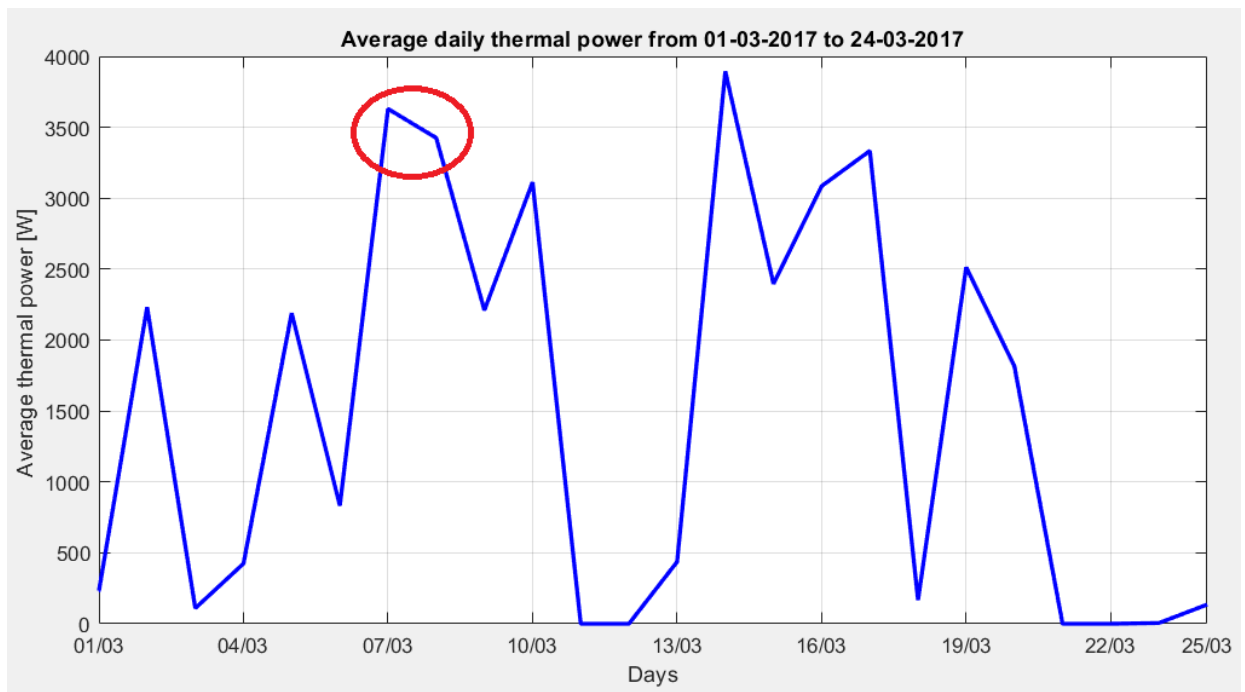


Figure 4.3: Average daily thermal power in March considering an 8-hour functioning period per day. Inside the red circle the data related to the days on which the daily analysis will be conducted.

Based on stable working conditions two days were taken to carry on the analysis on a daily basis, in order to choose these two days both a good average ΔT and the regularity of the produced thermal power were considered.

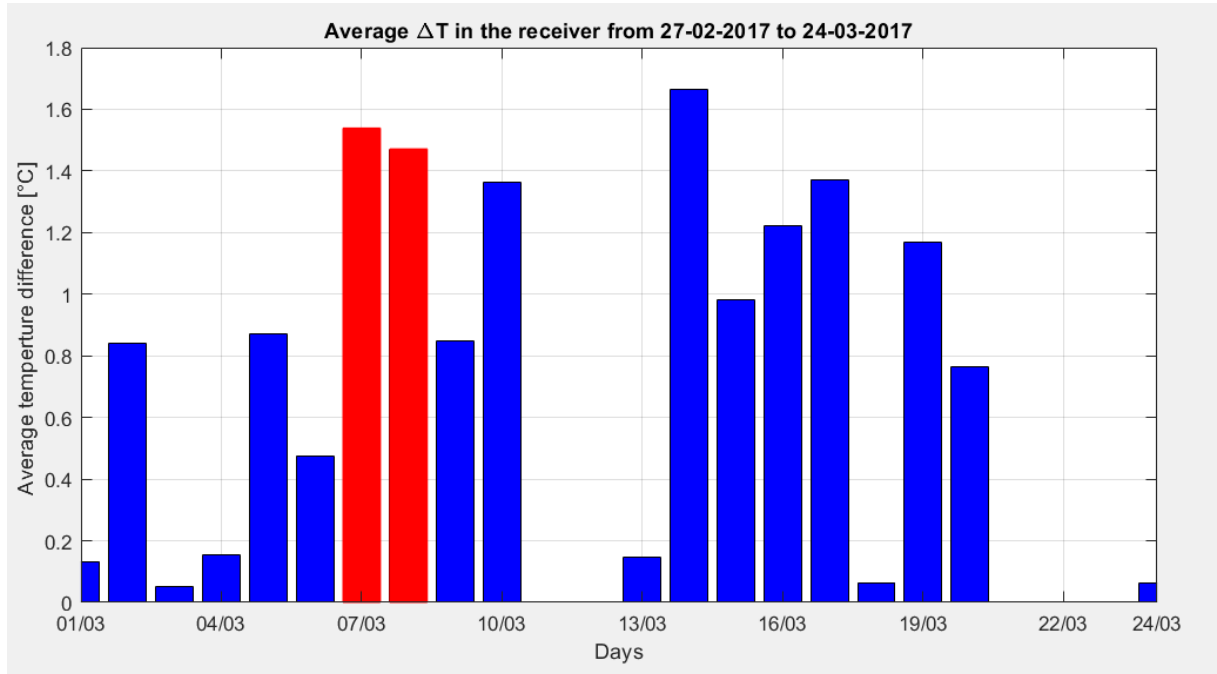


Figure 4.4: Average delta temperature in March. In red the data related to the days on which the daily analysis will be conducted.

In the following graphs main operating parameters are displayed, such as instantaneous thermal power, instantaneous efficiency and temperature difference between inlet and outlet.

- March 7, 2017

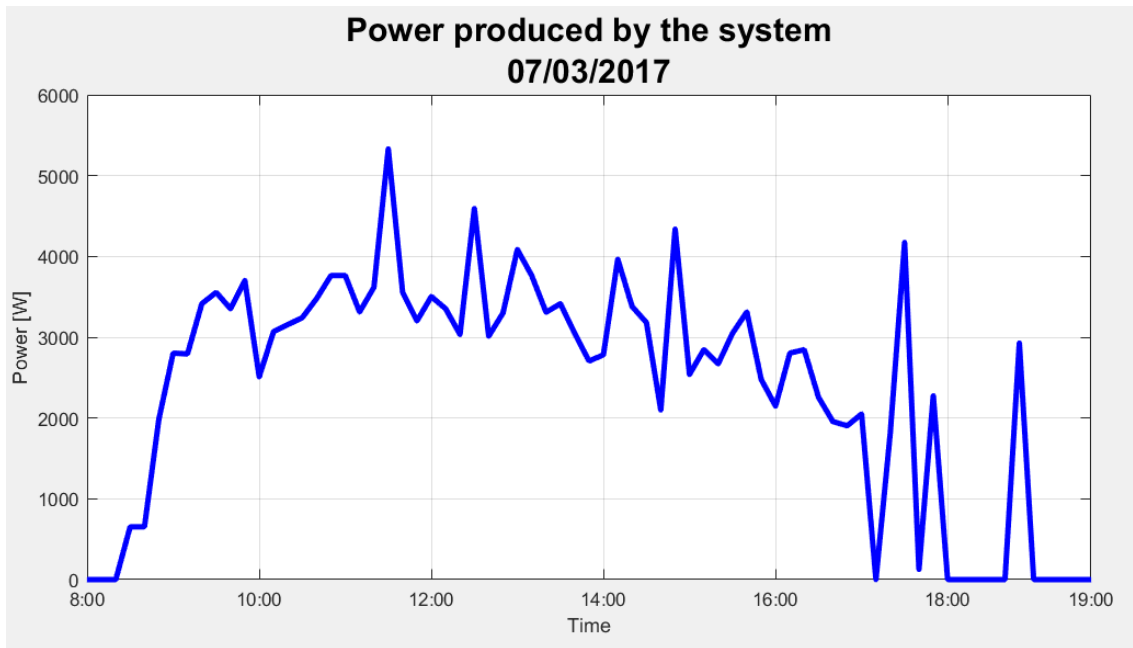


Figure 4.5: Thermal Power produced by the Turbocaldo system

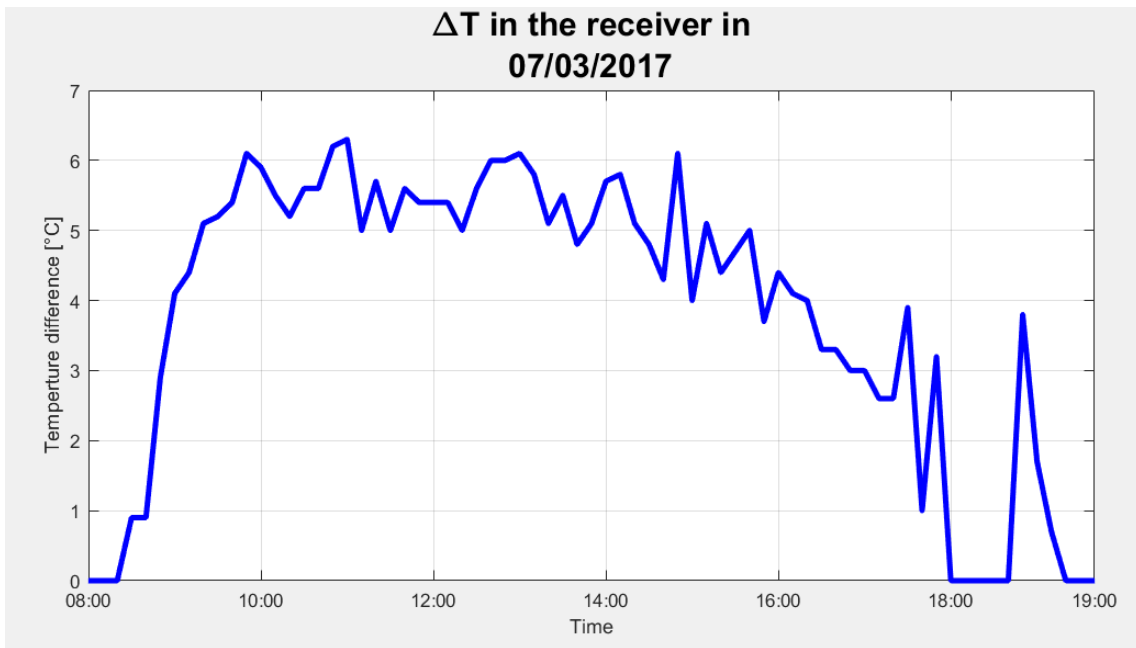


Figure 4.6: Temperature difference between inlet and outlet in the system.

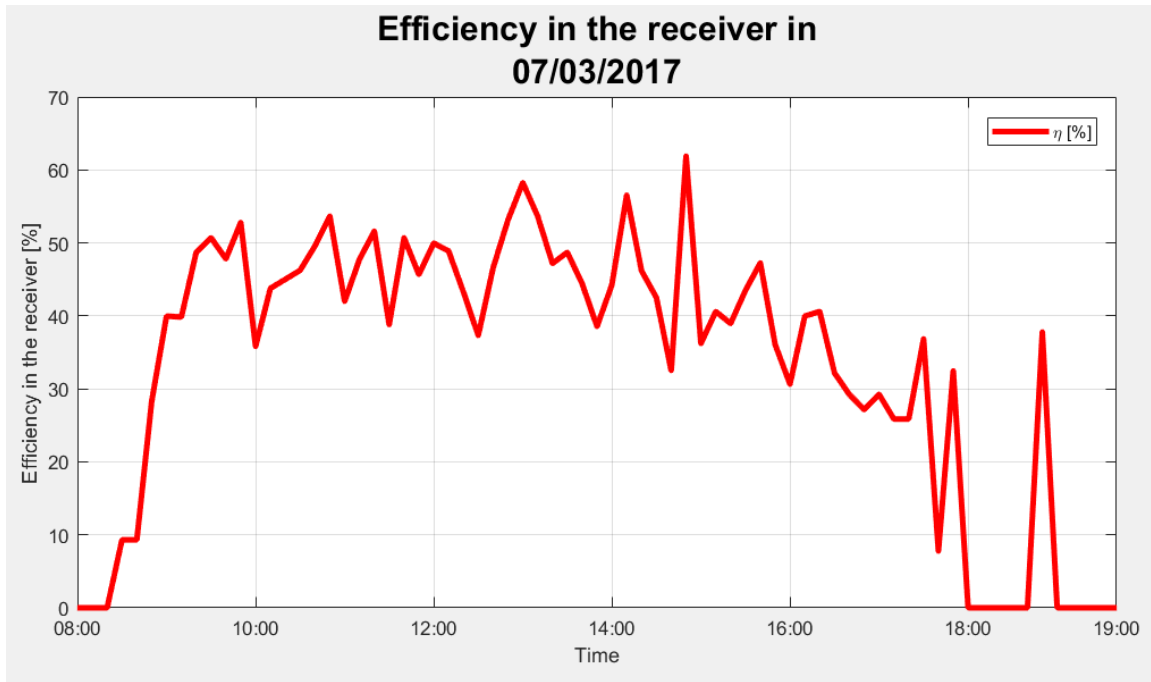


Figure 4.7: Instantaneous efficiency of the Turbocaldo system

As it was expected the trends of these three parameters are very similar, since they are all depending on the quantity of radiation entering the system. Indeed, the peaks and the best operating conditions occur in the middle of the day, while the system produces thermal power from around 8:00 a.m. to past 4:00 pm. The operating conditions of the system cause a raise in the boiler temperature which is directly proportional to the produced thermal power and therefore to the solar irradiance, in the working hours. The irradiance trend in March it is shown in figure.

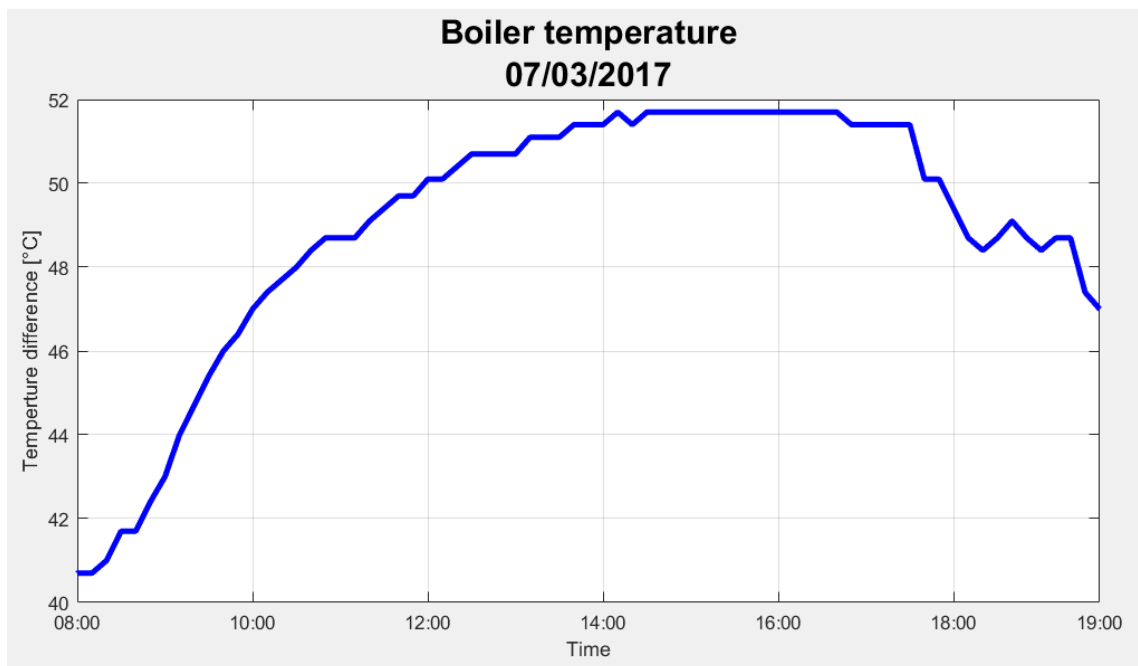


Figure 4.8: Boiler (or tank) temperature along the working hours of the system

-March 8, 2017

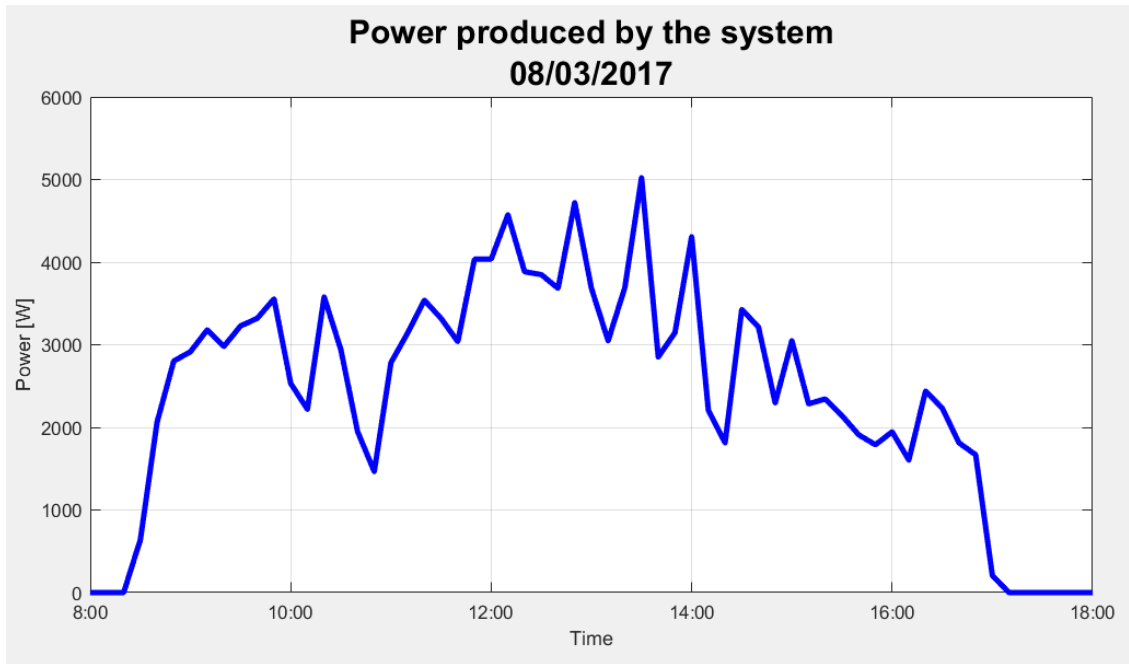


Figure 4.9: Thermal power produced by the Turbocaldo system

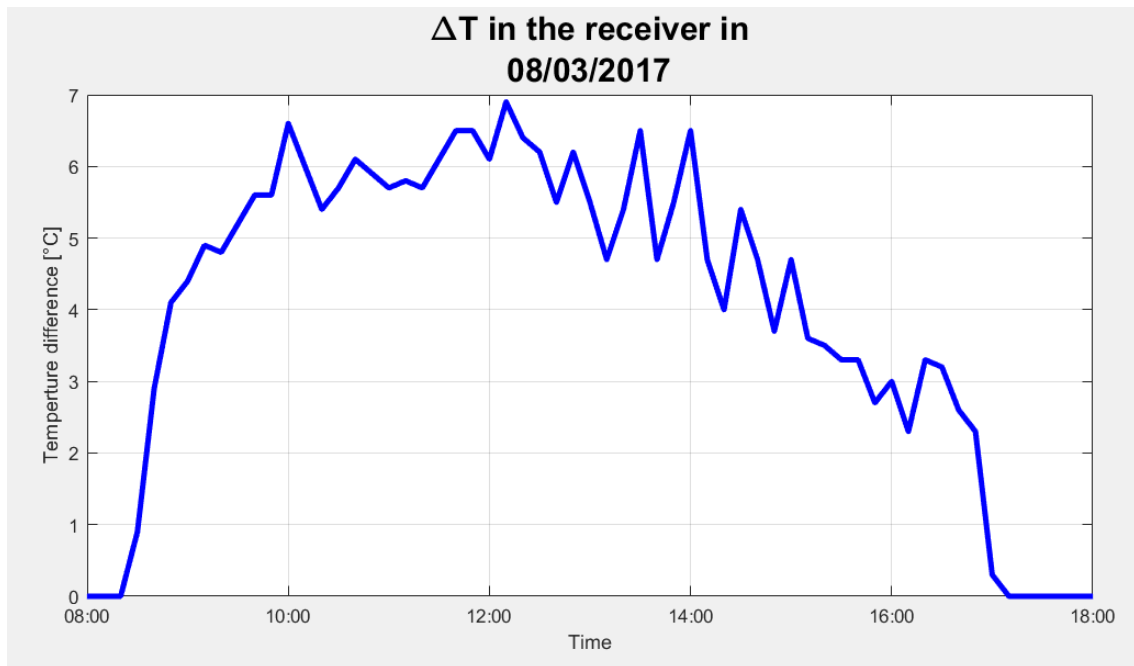


Figure 4.10: Temperature difference between inlet and outlet in the system.

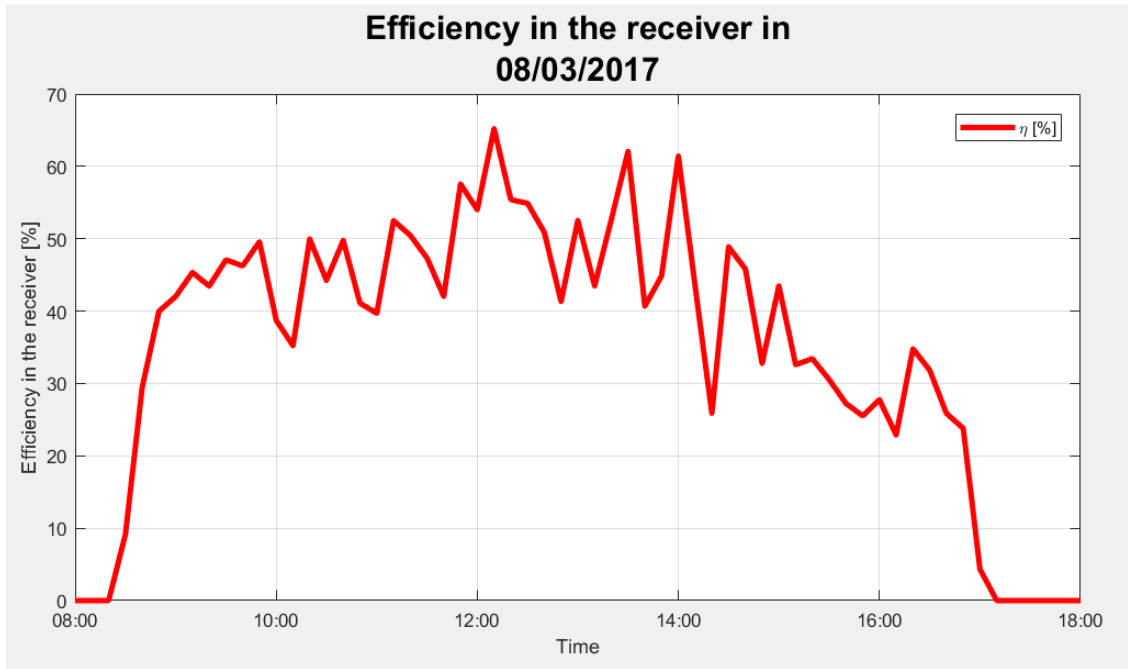


Figure 4.11: Instantaneous efficiency of the Turbocaldo system

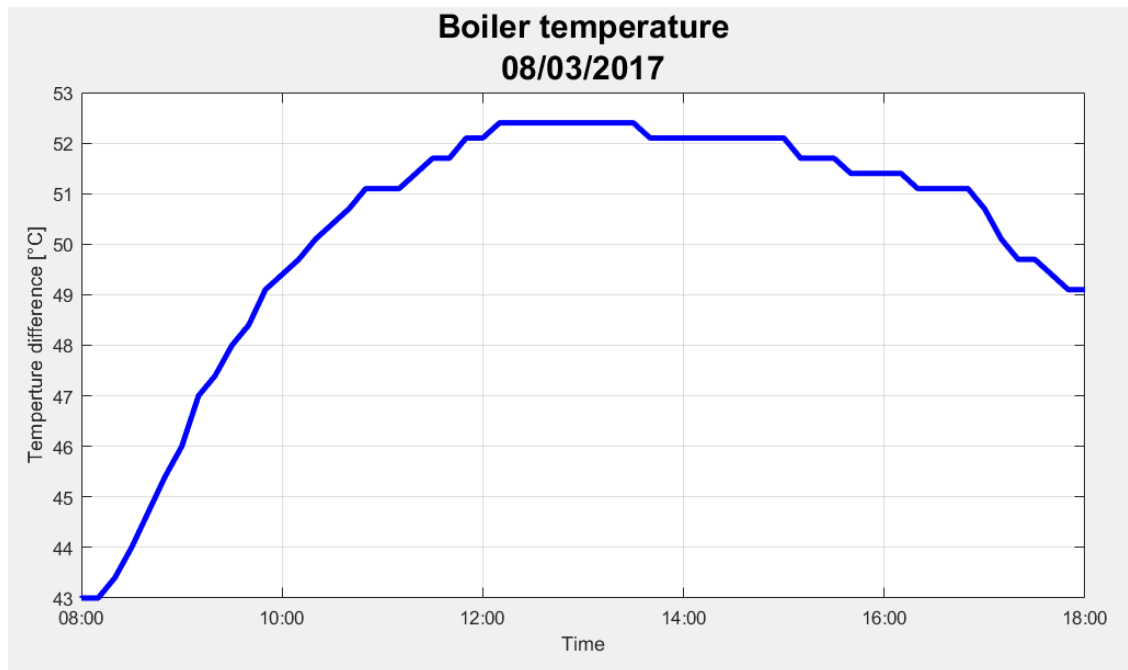


Figure 4.12: Boiler (or tank) temperature along the working hours of the system

It is evident that since the two days are close, and the irradiance is very similar, the trends of these parameters are very similar too, especially in terms of working hours. Despite this the trends are still different from each other, this may be due to clouds, wind or other external factors which are hard to predict with models.

Carrying on with the analysis, data belonging to the month of November were considered. As it can be seen in figure 4.1 The irradiance values for the month of

November are lower than in March, therefore we expect that a reduction also in the other parameters.

The following graphs show the trend of thermal power produced by the system and the average temperature difference between inlet and outlet throughout November 2017.

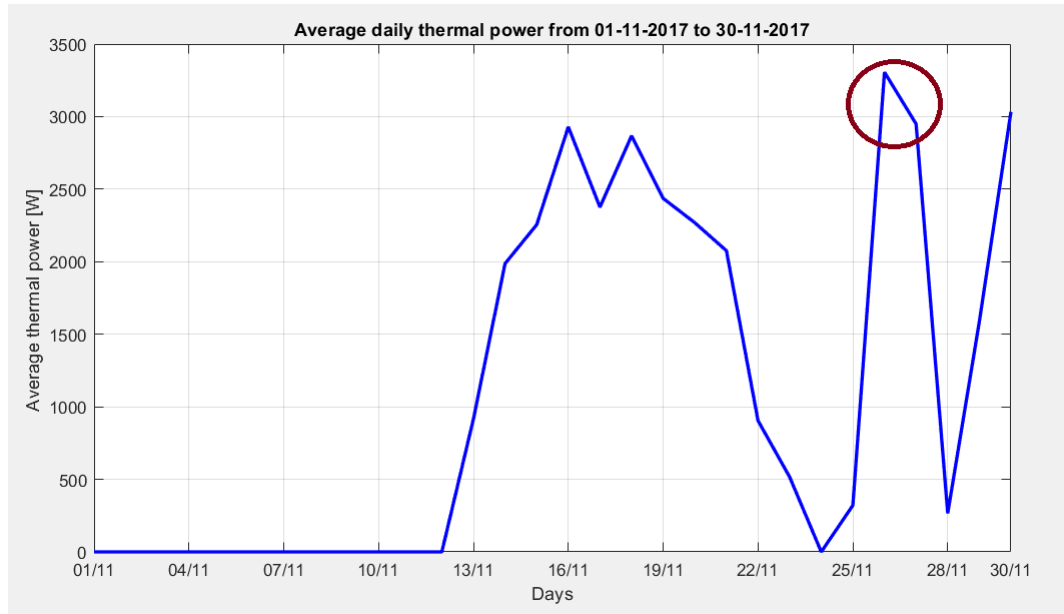


Figure 4.13: Average daily thermal power in November considering an 8-hour functioning period per day. Inside the red circle the data related to the days on which the daily analysis will be conducted

As done before two days are chosen in to analyze the system functioning on a daily basis, based on ΔT and thermal power production.

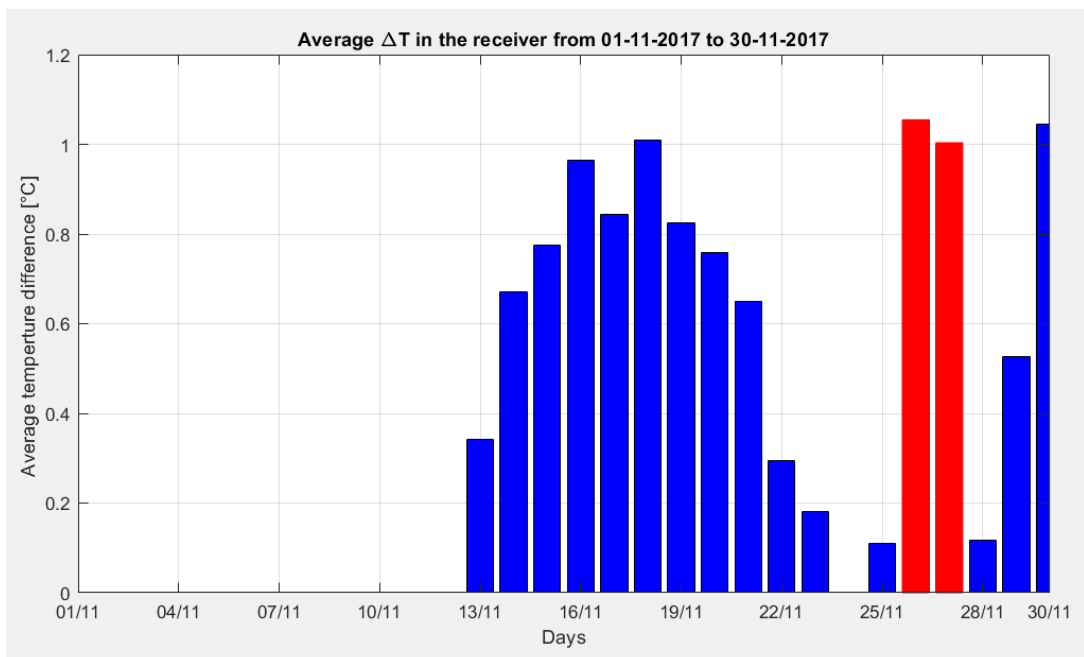


Figure 4.14: Average delta temperature in November. In red the data related to the days on which the daily analysis will be conducted

The analysis continues evaluating daily parameters variations.

- November 26, 2017

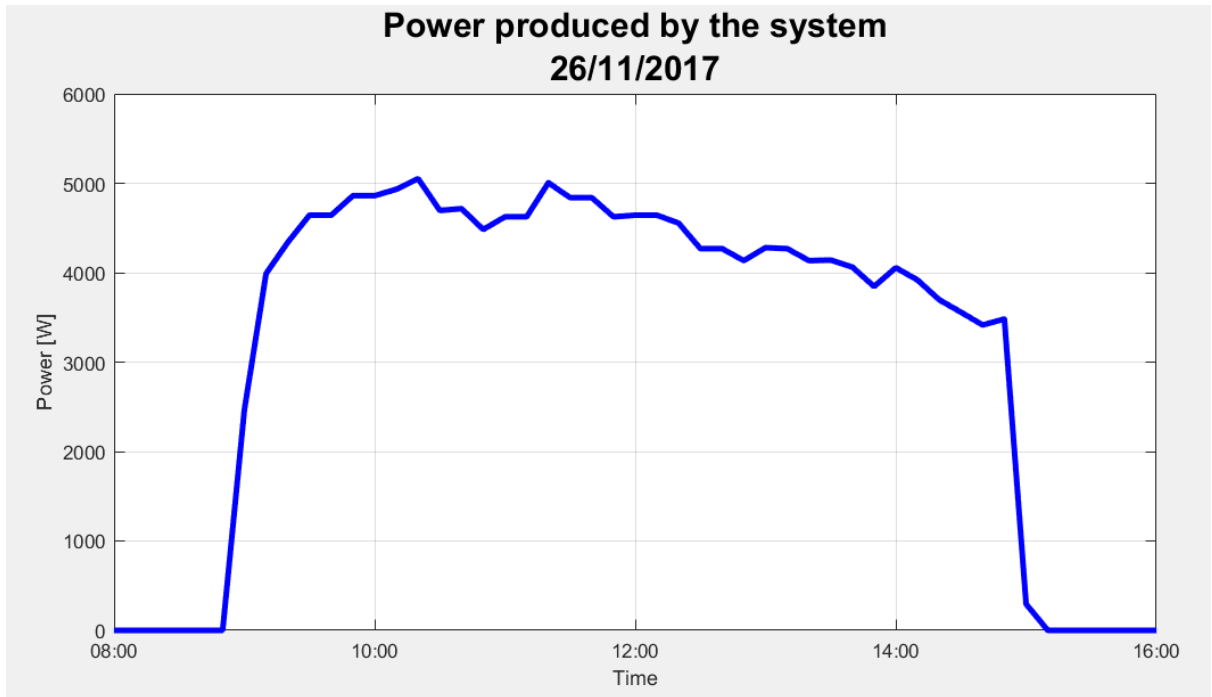


Figure 4.15: Thermal Power produced by the Turbocaldo system

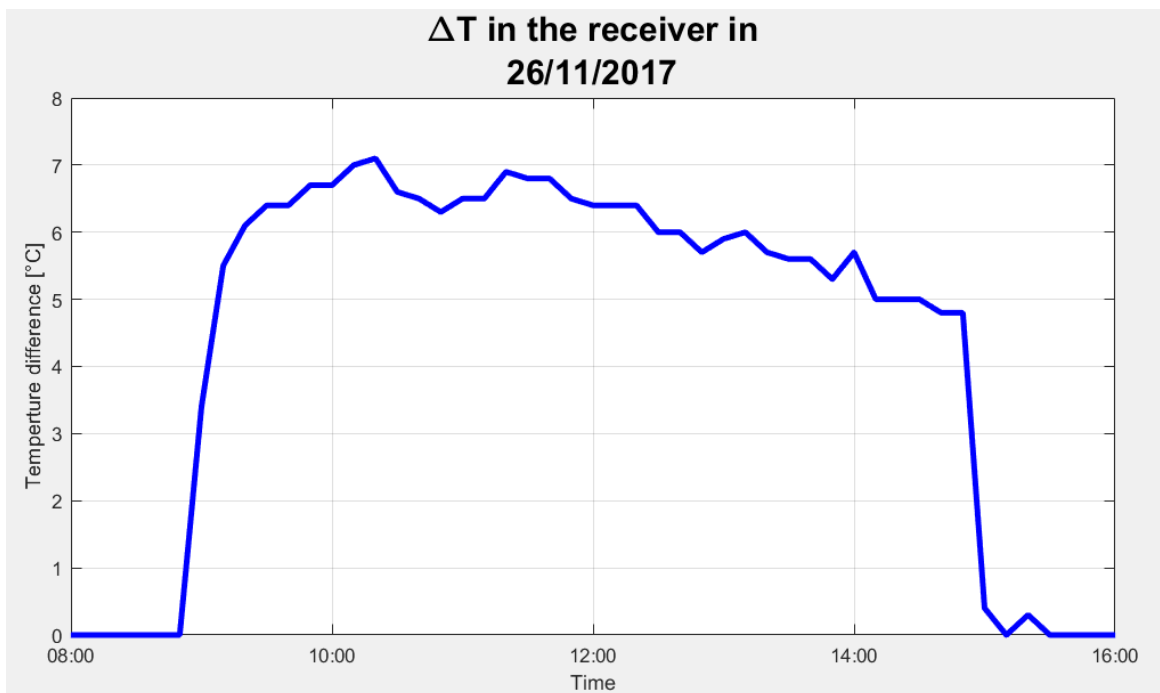


Figure 4.16: Temperature difference between inlet and outlet in the system.

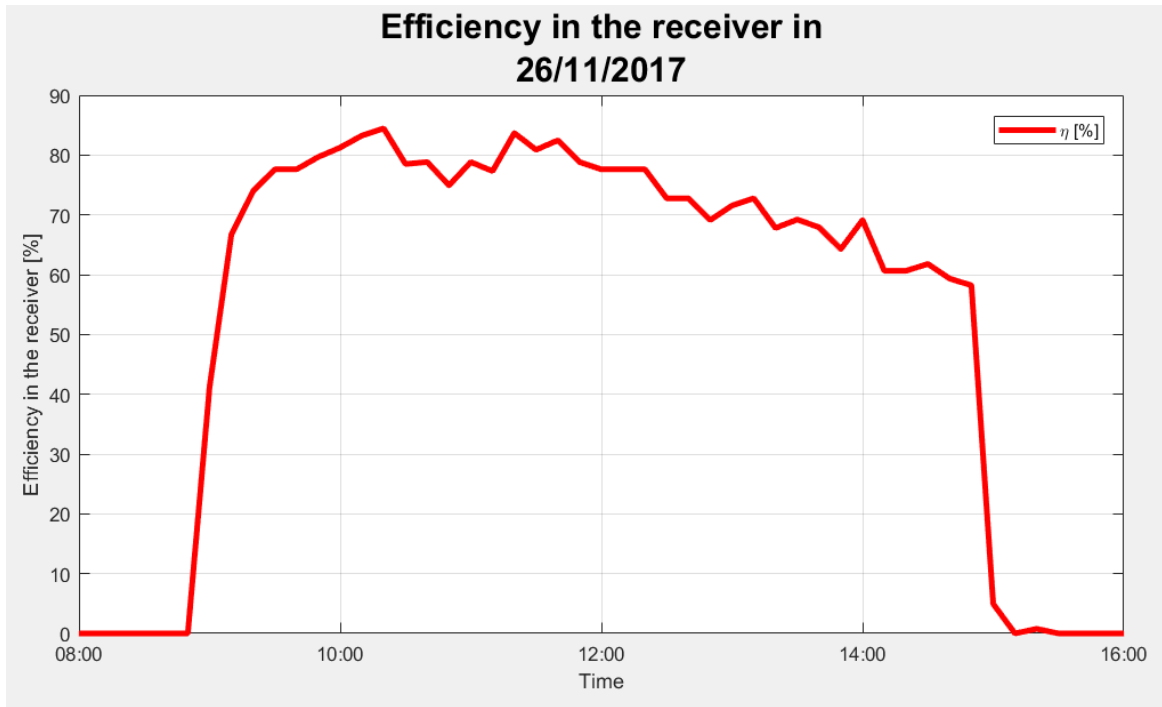


Figure 4.17: Instantaneous efficiency of the Turbocaldo system

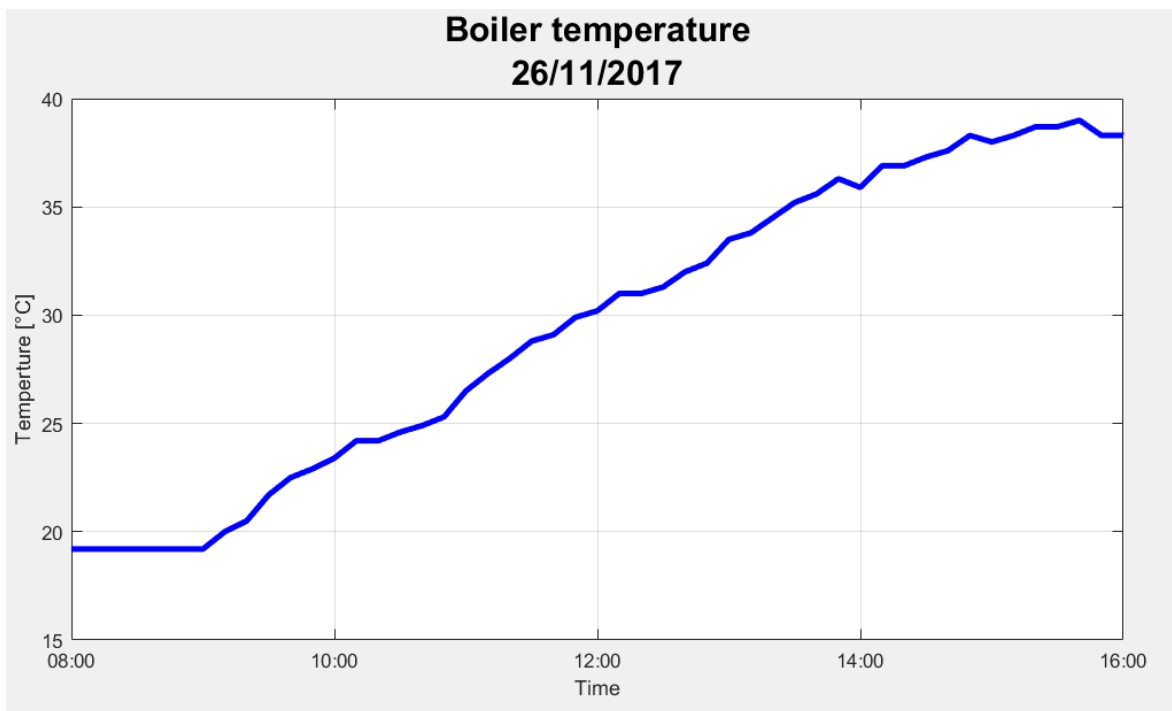


Figure 4.18: Boiler (or tank) temperature along the working hours of the system

- November 27, 2017

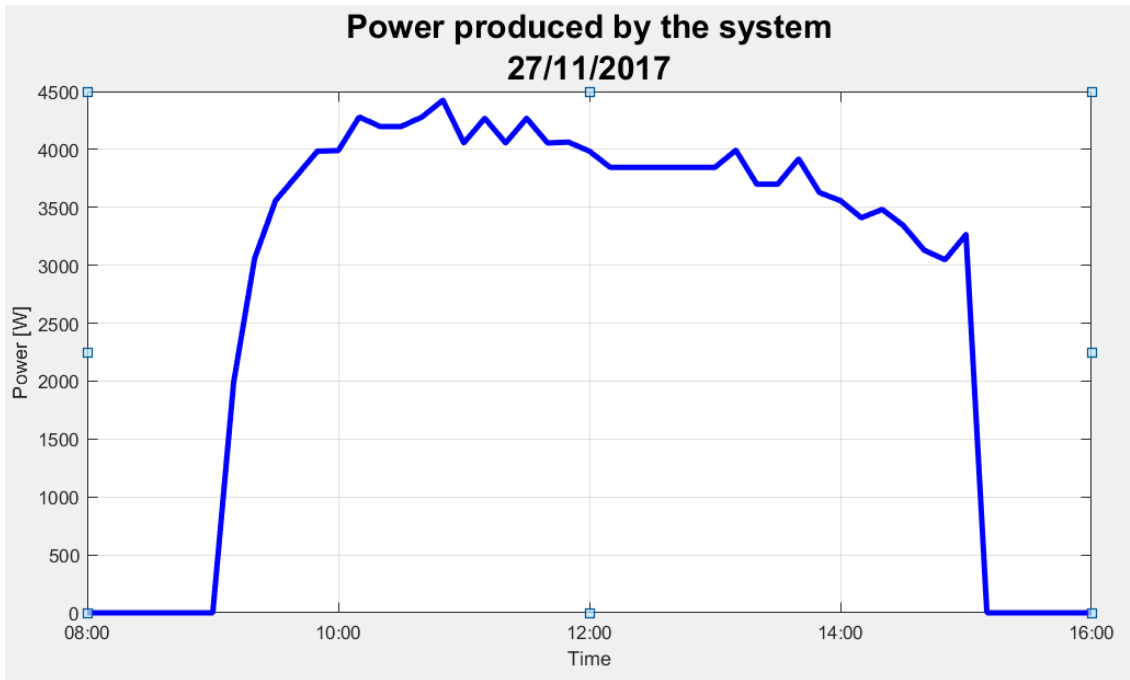


Figure 4.19: Thermal Power produced by the Turbocaldo system

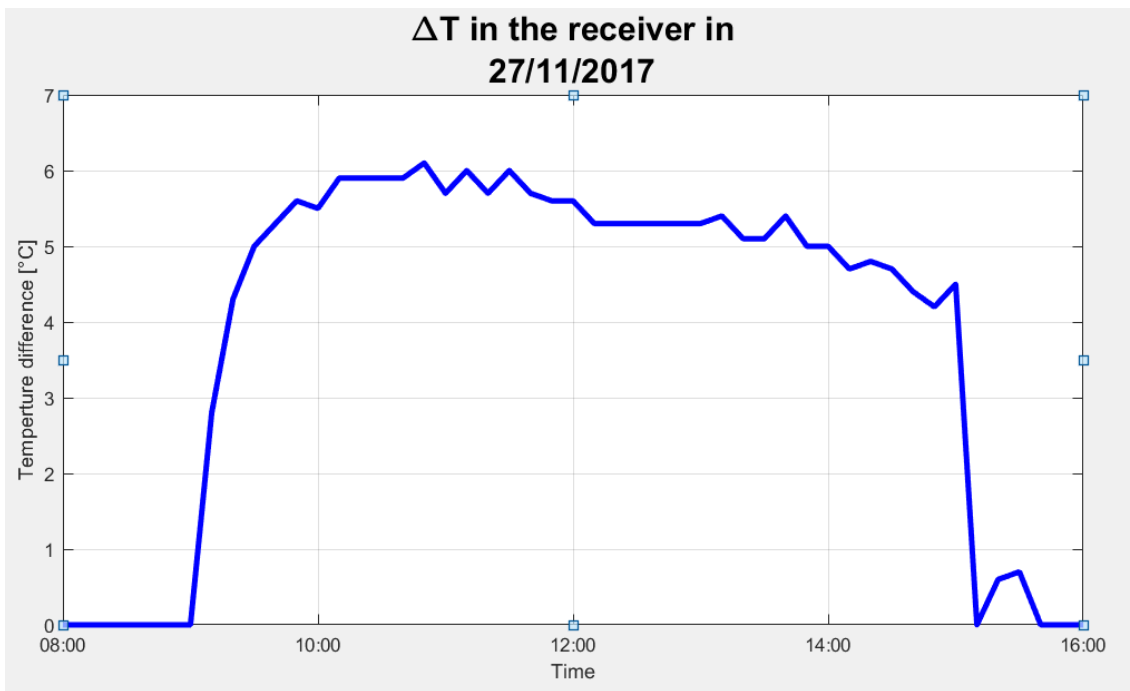


Figure 4.20: Temperature difference between inlet and outlet in the system.

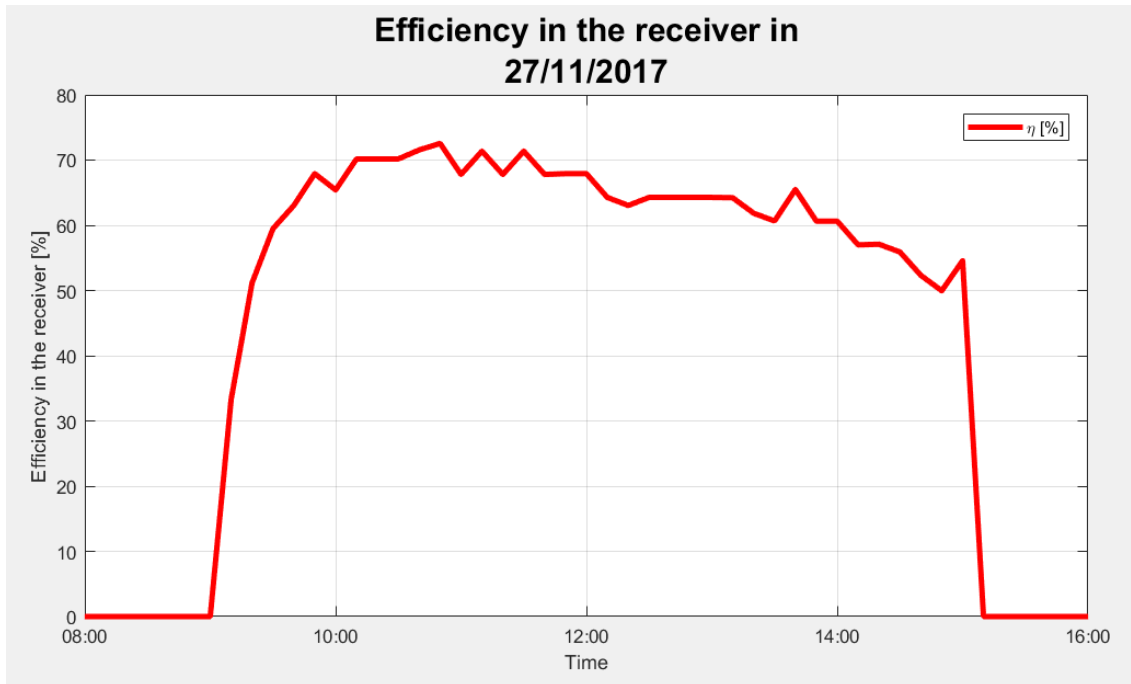


Figure 4.21: Instantaneous efficiency of the Turbocaldo system.

As it can be seen in figures 4.17 and 4.21, the efficiency, in this cases, is significantly higher with respect to the data for March 2017, this is due to the fact that we have similar productivity but in November the real-sky irradiance values are way lower than in March.

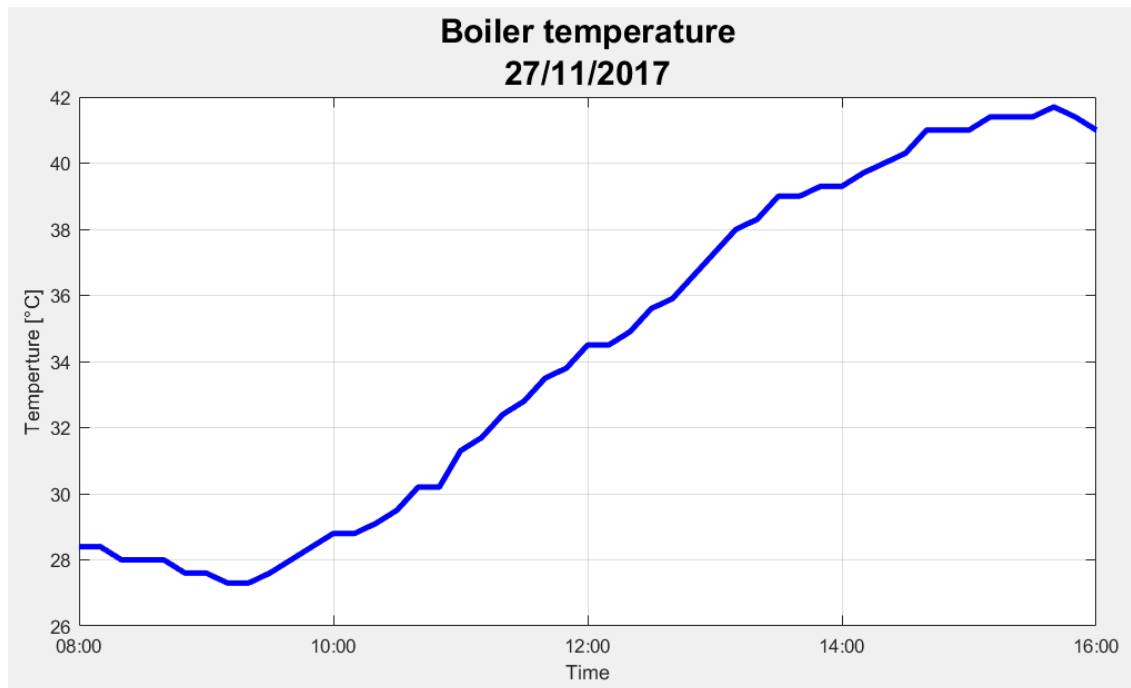


Figure 4.22: Boiler (or tank) temperature along the working hours of the system

In this day the trends are much more regular for every parameter and all considerations made for the previous cases are still valuable in this one. The last month analyzed is February 2018, as previously stated with the aim of comparing the results with the others, and to realize which are the current parameters and which is the current production of the system. Therefore, the following graphs display data concerning February 2018.

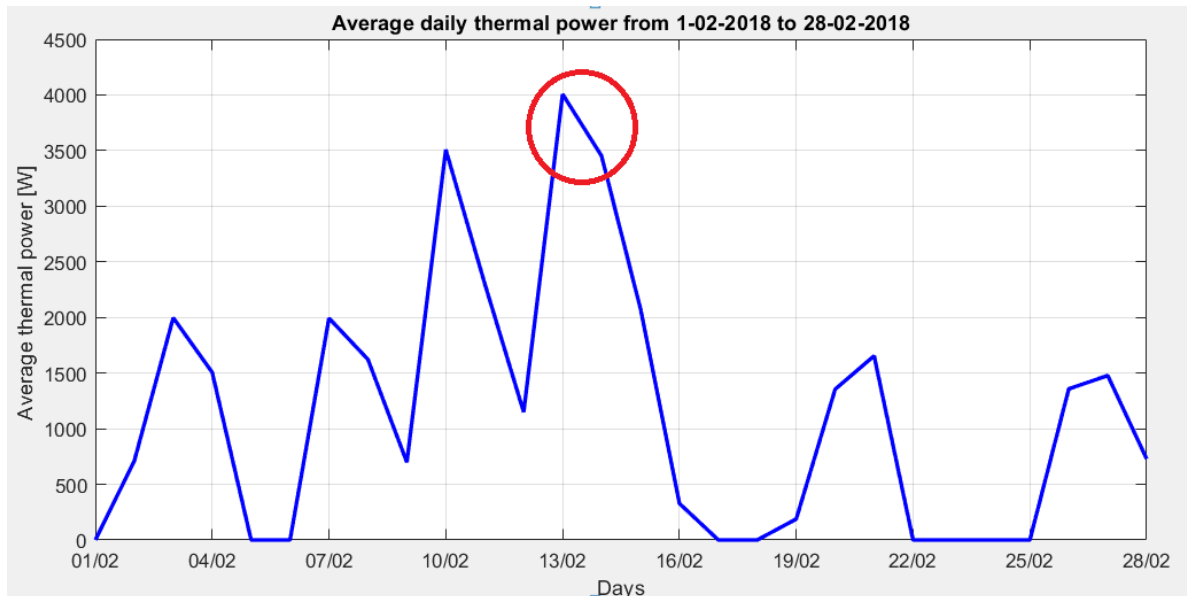


Figure 4.23: Average daily thermal power in February considering an 8-hour functioning period per day. Inside the red circle the data related to the days on which the daily analysis will be conducted

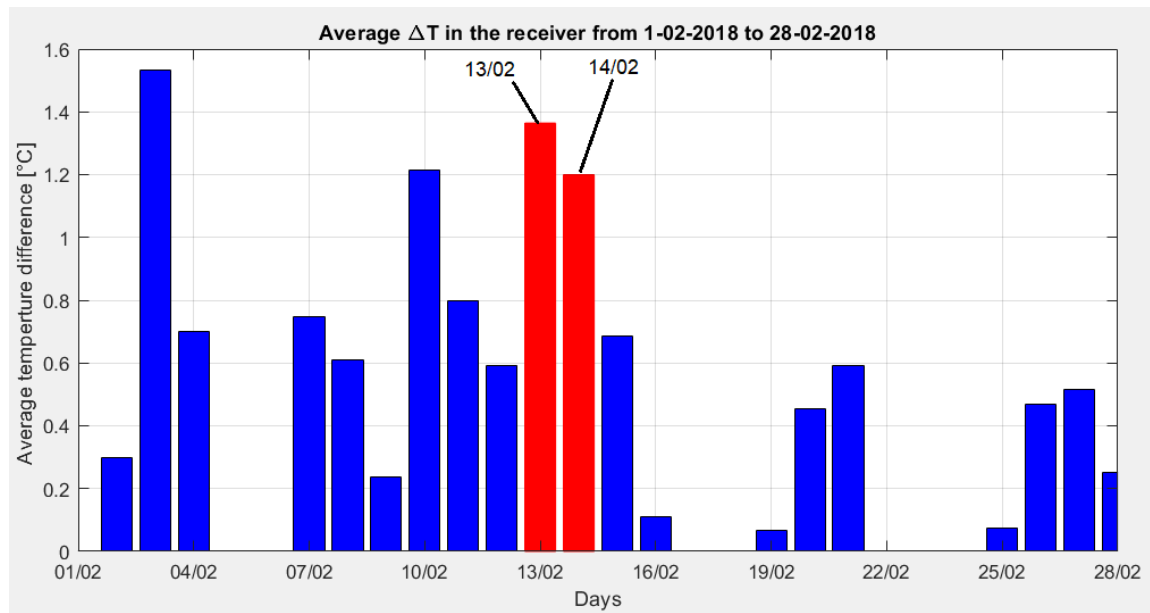


Figure 4.24: Average delta temperature in February. In red the data related to the days on which the daily analysis will be conducted

The analysis continues evaluating daily parameters variations.

- February 13, 2018

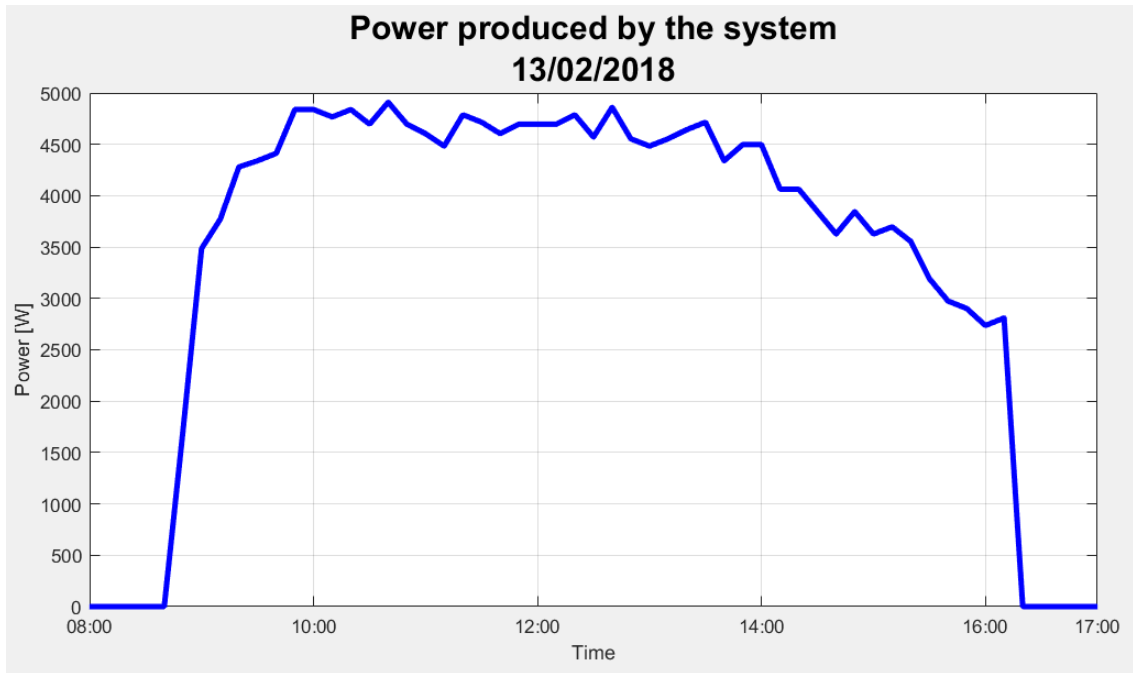


Figure 4.25: Thermal Power produced by the Turbocaldo system

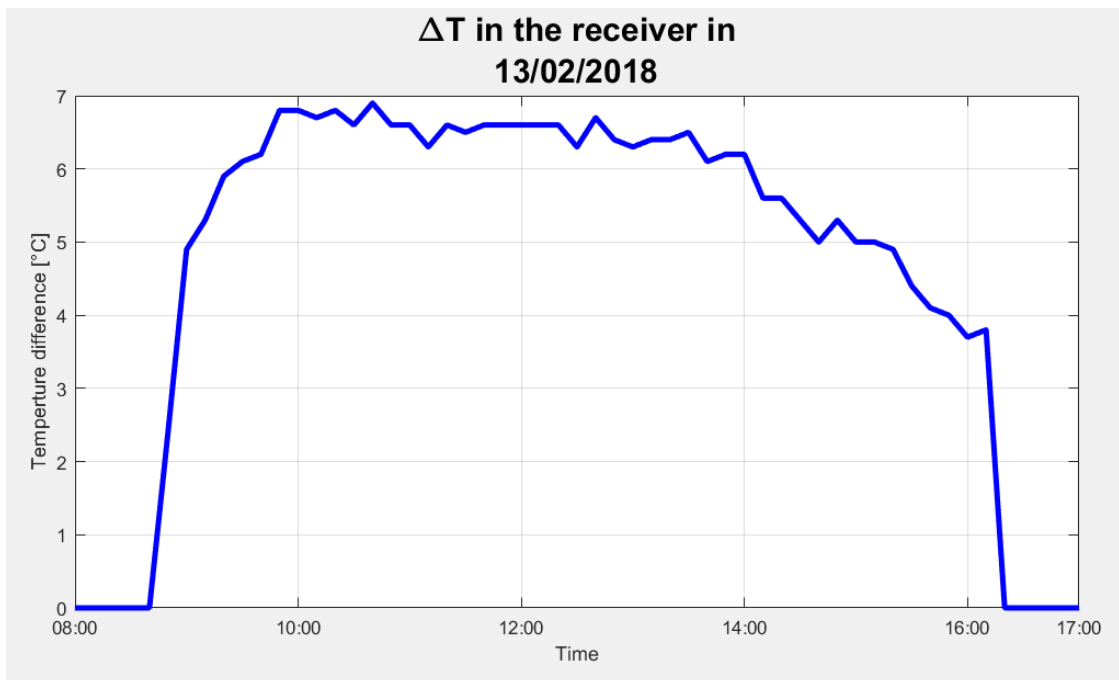


Figure 4.26: Temperature difference between inlet and outlet in the system.

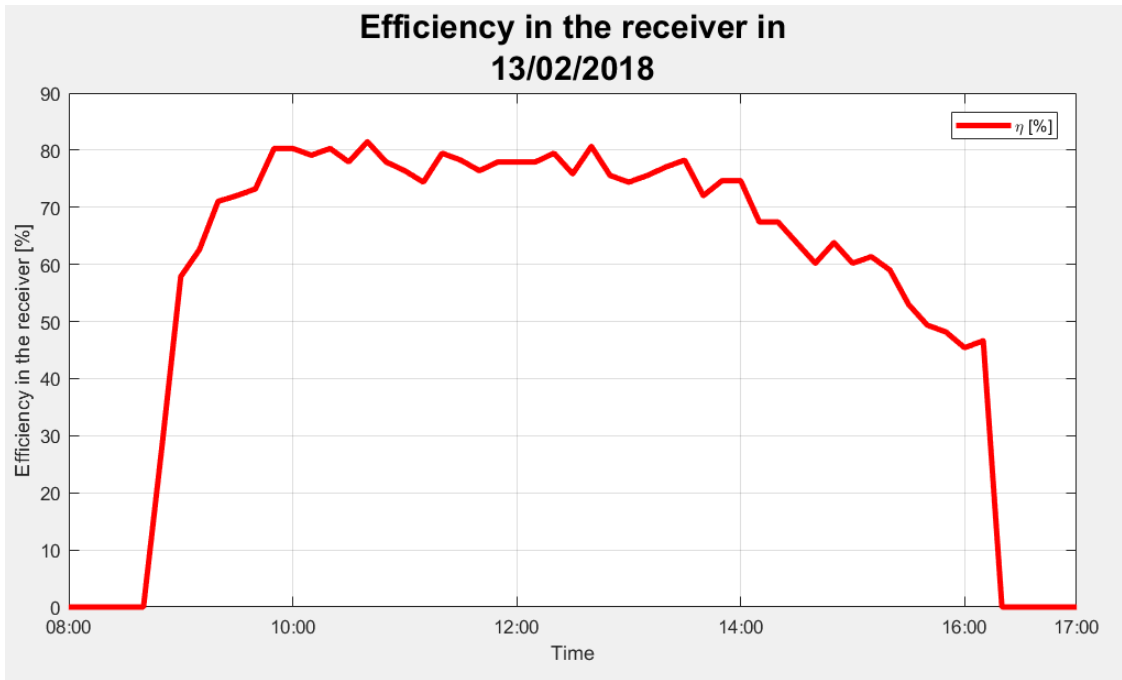


Figure 4.27: Instantaneous efficiency of the Turbocaldo system.

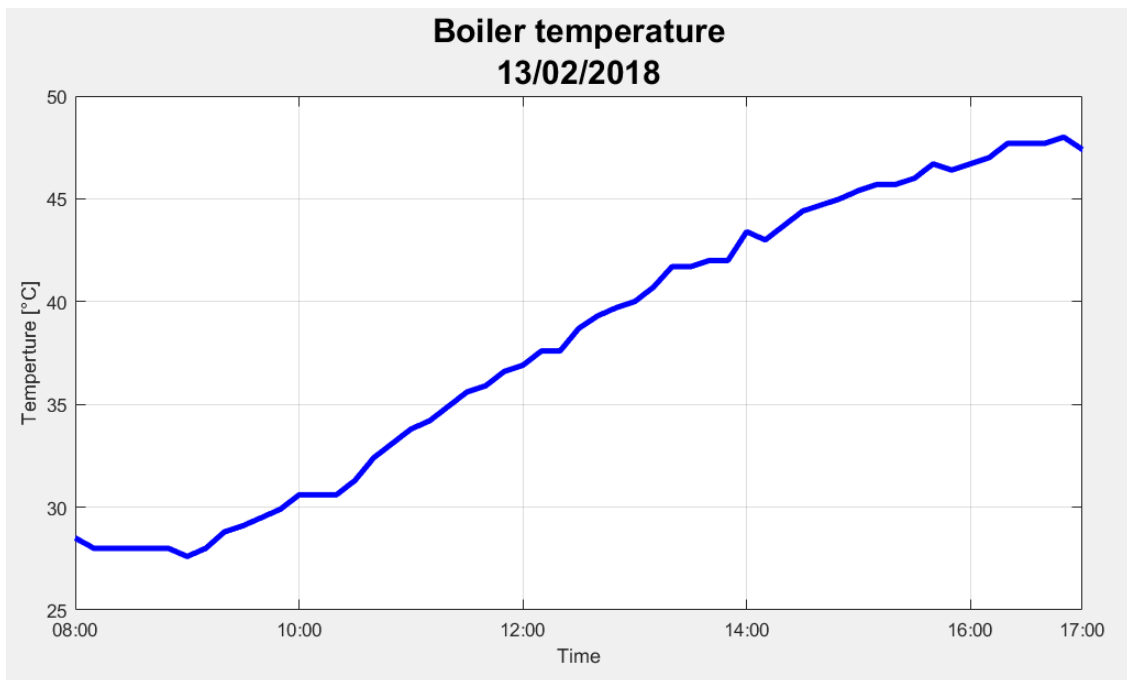


Figure 4.28: Boiler (or tank) temperature along the working hours of the system.

- February 14, 2018

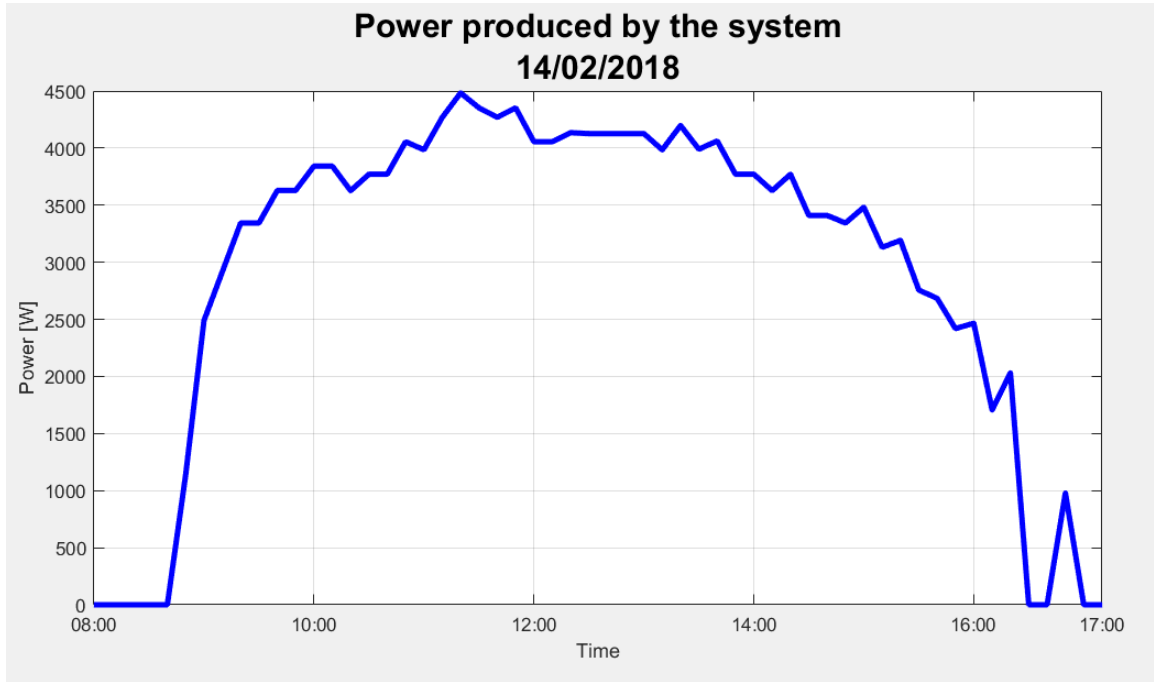


Figure 4.29: Thermal Power produced by the Turbocaldo system

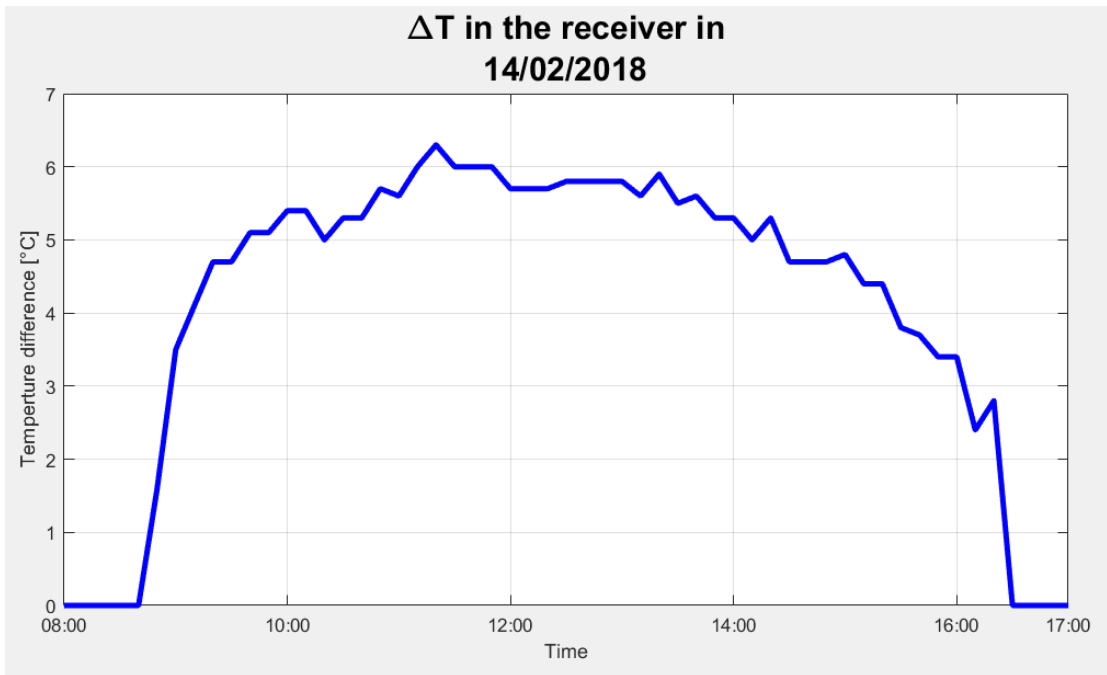


Figure 4.30: Temperature difference between inlet and outlet in the system.

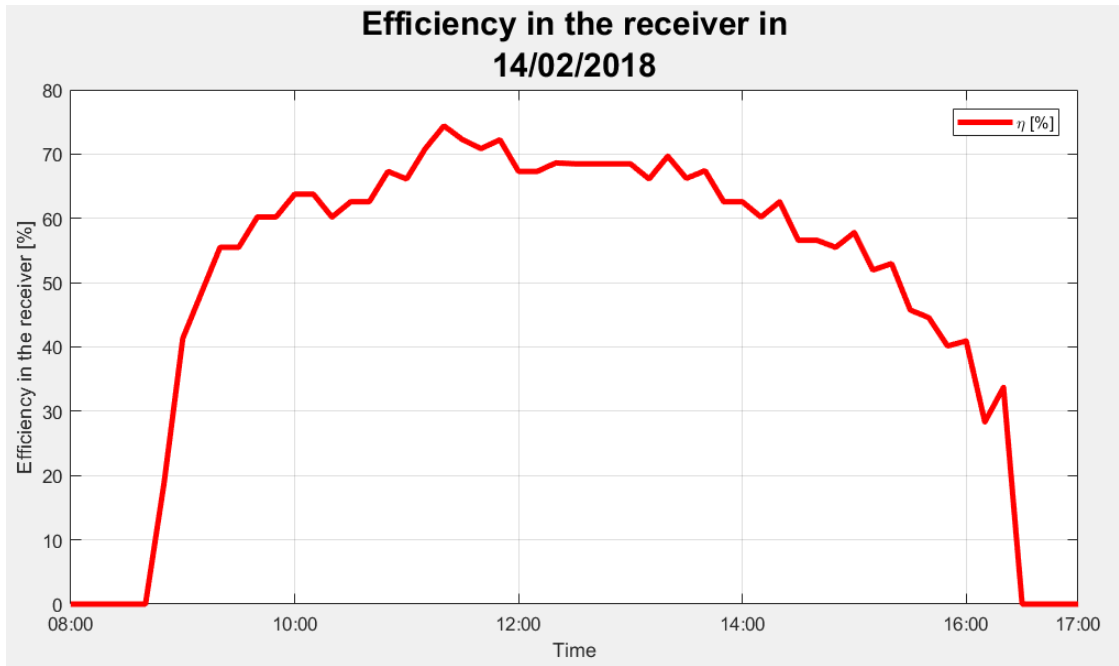


Figure 4.31: Instantaneous efficiency of the Turbocaldo system.

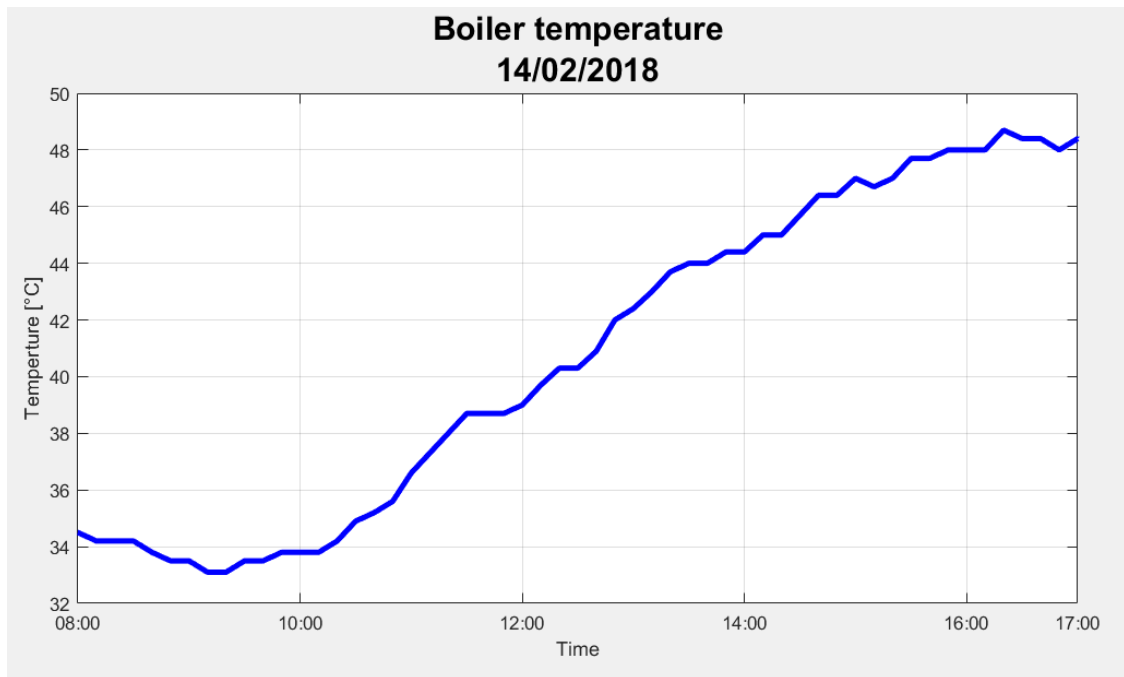


Figure 4.32: Boiler (or tank) temperature along the working hours of the system.

As it may be seen the production in the two days is very similar, as well as with respect to the past year. The production is linear throughout the day and efficiencies reach a good level (figures 4.31 and 4.27), with values similar to November 2017 and therefore higher than March 2017. This is due to the fact that with high values of real-sky irradiance, high productivity levels are reached.

4.5 Modelling of the receiver

The software COMSOL Multiphysics was exploited for building up a model of the system's receiver, with the aim of checking with experimental data the validity of the model to predict its functioning having only the direct irradiance in input.

The measures were taken by hand and therefore a tolerance of ± 0.1 cm must be taken into account.

4.5.1 The model

First the geometry of the model is built up representing the receiver in all its components, then some assumptions are made in order to reduce computational cost and optimize simulations.

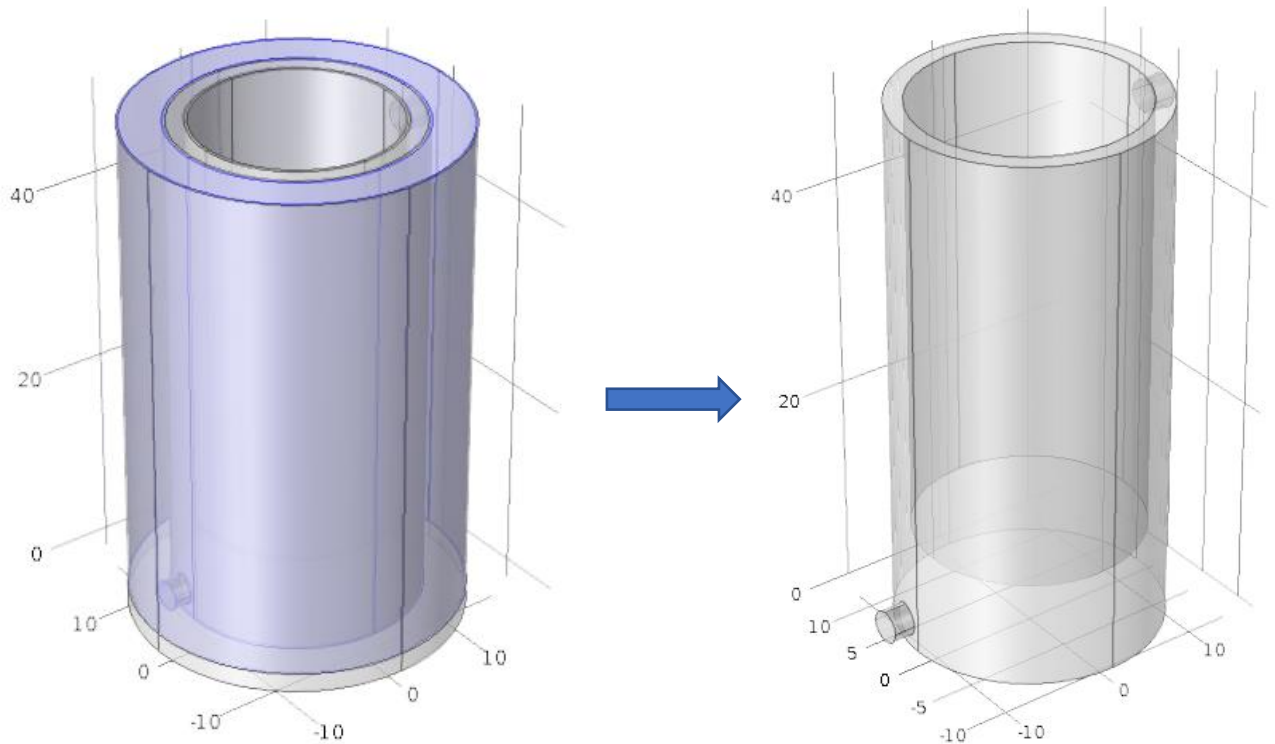


Figure 4.33: Geometry of the Turbocaldo model (left. complete, right. simplified)

In this case the external layer of rock wool is substituted with a convective boundary condition, which must take into account all the thermal losses with the environment, mitigated by the insulant. The internal steel layer may be removed due to the negligible thermal conductivity with respect to the water one.

Once the geometry is ready, materials and physics must be set. In our case, water is the involved material, two physics take place, in detail: heat transfer and turbulent flow.

- Heat Transfer:

Settings for heat transfer include initial values, heat transfer with solids and fluids and boundary conditions. As said before, an external boundary condition is set to take into account thermal losses with the environment, where the heat transfer coefficient is found summing the component for external losses and the component due to the insulant.

Convective heat flux
 $q_0 = h \cdot (T_{\text{ext}} - T)$
 Heat transfer coefficient:
 User defined
 Heat transfer coefficient:
 h 1000 W/(m²·K)
 External temperature:
 T_{ext} 293.3[K] K

Figure 4.34: Settings for external thermal losses.

Other fundamental boundary conditions are the boundary heat source which represents the solar radiation conveyed into the receiver by the solar dish. Data in this setting are taken from PV GIS as previously stated.

Boundary Selection
 Selection: Manual
 ON
 Active: 11, 12, 15, 16
 Override and Contribution
 Equation
 Boundary Heat Source
 General source
 Q_b User defined
 5260.302 W/m²

Figure 4.35: Settings for radiation input condition

- Turbulent flow

Settings for turbulent flow include info on the physical model:

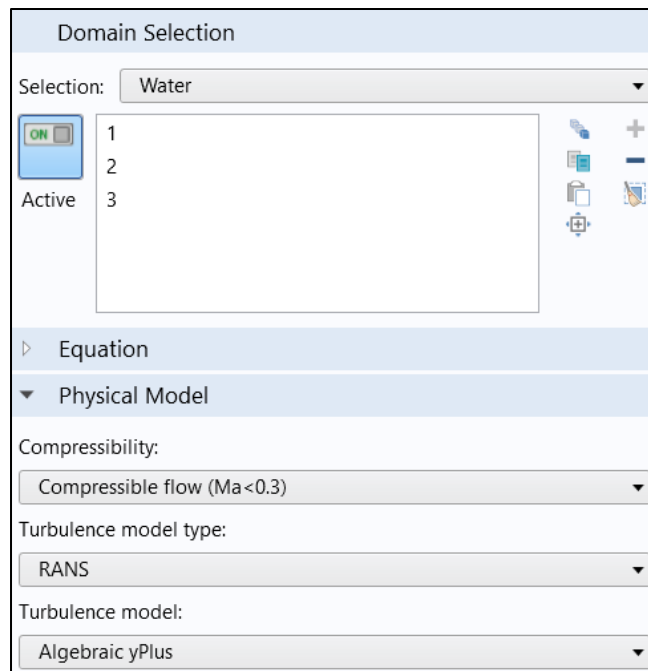


Figure 4.36: Settings for Turbulent Flow physics.

Other settings are for defining inlet mass flow rate (around 0.167 kg/s in our application) and outlet relative pressure (which must be null).

4.5.2 Check with experimental data

After building up the model itself is fundamental to check the validity of its results. To achieve this goal, the experimental results are used. To reduce the computational cost, stationary behavior is investigated; therefore, some simplification must be performed. In order to fulfill our requests, it is necessary:

- Definition of a working period,
- Definition of the initial conditions (in terms of temperature, mass flow rate),
- Definition of an average irradiance entering the system in the functioning period, both clear-sky and real-sky condition,
- Definition of average external conditions during the functioning,
- Definition of the average mass flow rate during the functioning.

Since the situation is based on experimental data real-sky irradiation must be used, and an optical efficiency must be added to the irradiance to take in to account problems due to dirt and dust on the reflector and other optical losses.

The first evaluated day is March 7, 2017.

	hours [h]	Cool In T [°C]	Cool Out T [°C]	Delta T [°C]	T Ambiente [°C]	Flow rate (kg/s)	CSI [W/m2]	RSI [W/m2]
07-mar-17	(8-16)	53,6	58,7	5,1	20,6	0,1492	687,2	468,2

Table 4.1: data for March 7, 2017

All these data are then included in the model and the simulation is run. The results of the simulation are displayed in the following figures.

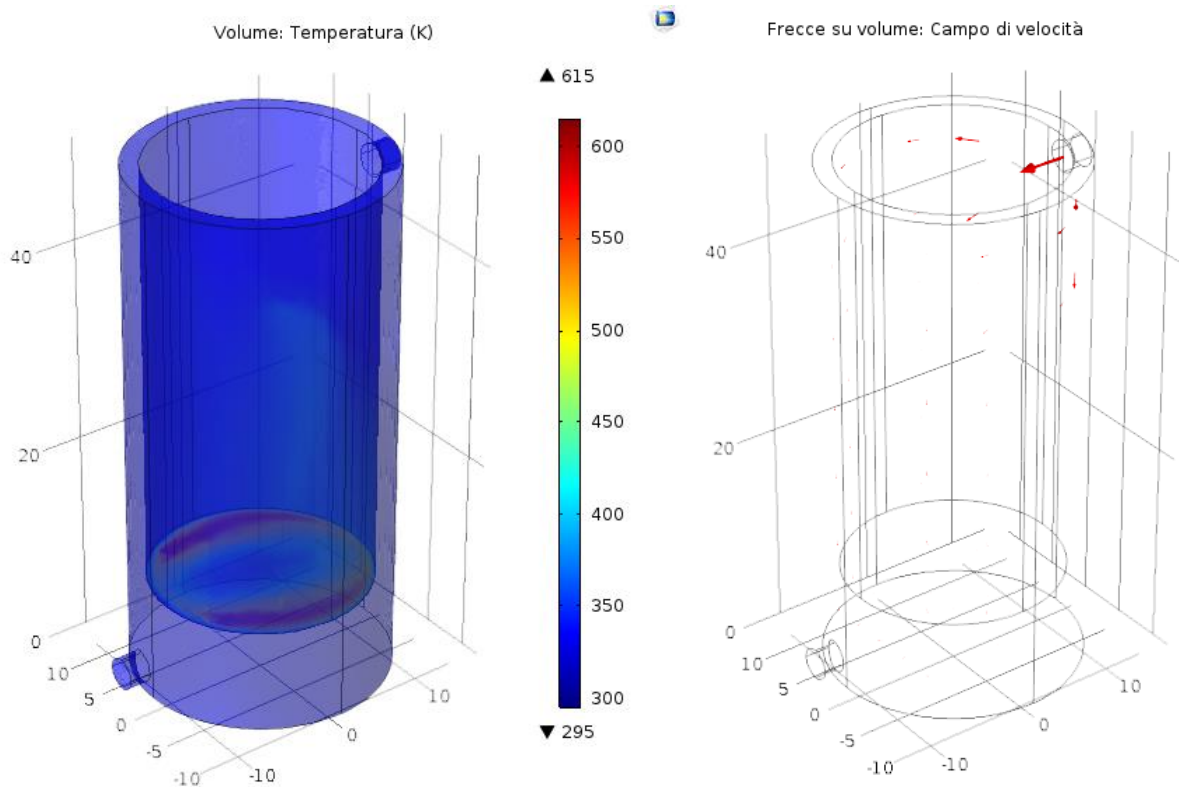


Figure 4.37: temperature and velocity profile in the Turbocaldo system for March 7, 2017

It is our interest to evaluate the temperature at the outlet of the system and the temperature difference between inlet and outlet. From the velocity profile, which is nearly the same for every simulation, the flow of the fluid inside the receiver can be tracked, the mass flow rate can be considered constant from inlet to outlet.

The results obtained from the simulation are displayed in the following table:

	hours [h]	Cool In T [°C]	Experimental CO T [°C]	Experimental ΔT [°C]	Model CO T [°C]	Model ΔT [°C]	Error [%]
07-mar-17	(8-16)	53,6	58,7	5,1	59,0	5,4	5,3

Table 4.2: Results March 7, 2017

Next day taken into analysis is March 8,2017:

	hours [h]	Cool In T [°C]	Cool Out T [°C]	Delta T [°C]	T Ambiente [°C]	Flow rate (kg/s)	CSI [W/m2]	RSI [W/m2]
08-mar-17	(8-16)	51,5	57,0	5,5	22,4	0,1478	687,2	468,2

Table 4.3: data for March 8, 2017

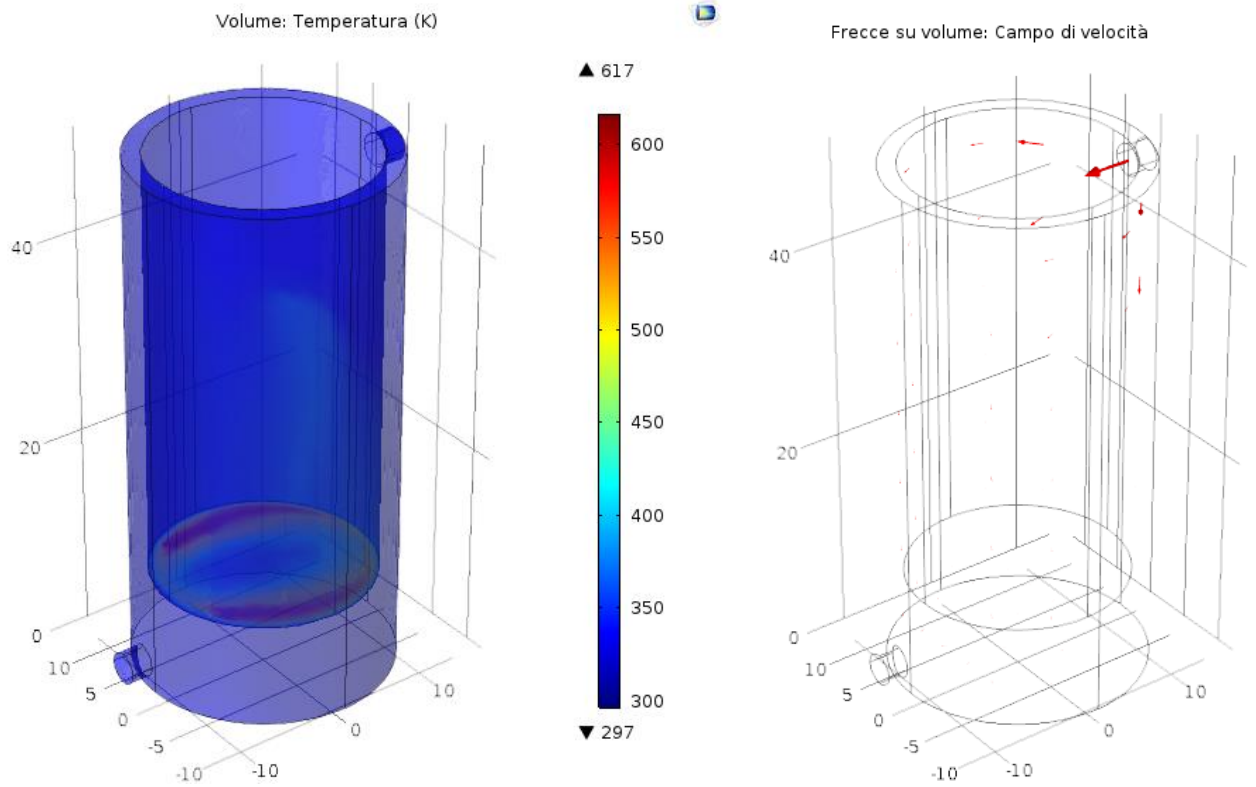


Figure 4.38: temperature and velocity profile in the Turbocaldo system for March 7, 2017

The simulation was set as previously, and the results are displayed in the following table:

	hours [h]	Cool In T [°C]	Experimental CO T [°C]	Experimental ΔT [°C]	Model CO T [°C]	Model ΔT [°C]	Error [%]
08-mar-17	(8-16)	51,5	57,0	5,5	57,7	6,2	12,5

Table 4.4: Results for March 8,2017

Next simulations were conducted throughout the month of November.
 Next day taken into analysis is November 26, 2017:

	hours [h]	Cool In T [°C]	Cool Out T [°C]	Delta T [°C]	T Ambiente [°C]	Flow rate (kg/s)	CSI [W/m ²]	RSI [W/m ²]
26-nov-17	(9-13)	34,4	40,2	5,8	21,6	0,1730	651,8	308,5

Table 4.5: data for November 26, 2017

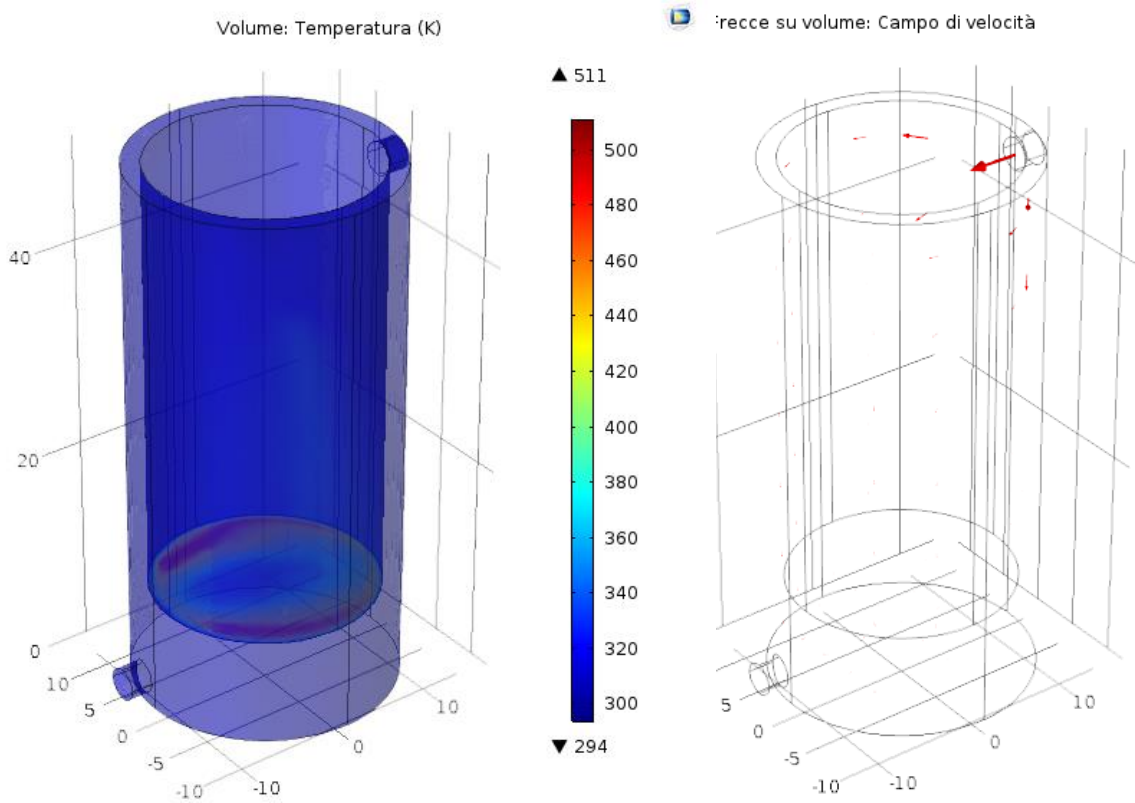


Figure 4.39: temperature and velocity profile in the Turbocaldo system for November 14, 2017

The outcome results are displayed in the following table:

	hours [h]	Cool In T [°C]	Experimental CO T [°C]	Experimental ΔT [°C]	Model CO T [°C]	Model ΔT [°C]	Error [%]
26-nov-17	(9-13)	34,4	40,2	5,8	39,8	5,4	7,5

Table 4.6: Results for November 26,2017

Next day taken into analysis is November 27, 2017:

	hours [h]	Cool In T [°C]	Cool Out T [°C]	Delta T [°C]	T Ambiente [°C]	Flow rate (kg/s)	CSI [W/m ²]	RSI [W/m ²]
27-nov-17	(9-13)	40,0	45,3	5,3	23,3	0,1713	651,8	308,5

Table 4.7: data for November 27, 2017

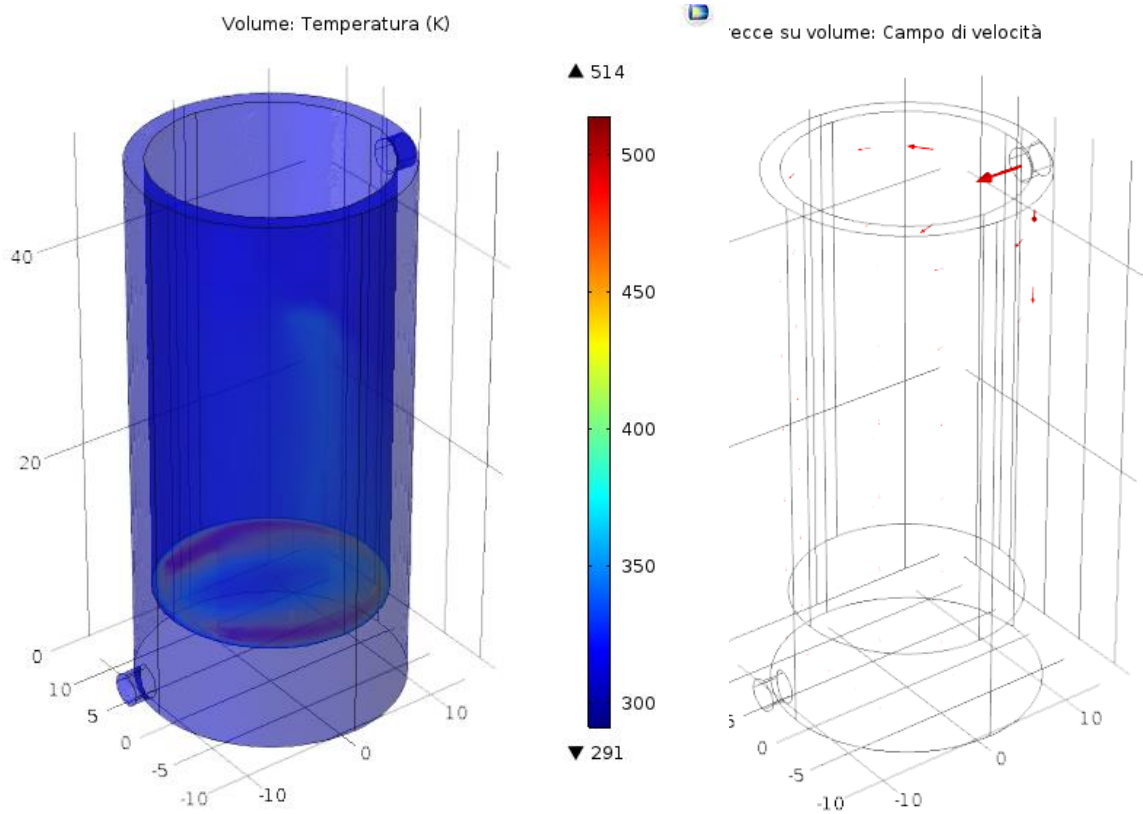


Figure 4.40: temperature and velocity profile in the Turbocaldo system for November 15, 2017

The outcome results are displayed in the following table:

	hours [h]	Cool In T [°C]	Experimental CO T [°C]	Experimental ΔT [°C]	Model CO T [°C]	Model ΔT [°C]	Error [%]
27-nov-17	(9-13)	40,0	45,3	5,3	44,6	4,6	12,2

Table 4.8: Results for November 27, 2017

In order to have an idea on the actual performances of the system the next simulations were conducted throughout the month of February.

Next day taken into analysis is February 13, 2018:

	hours [h]	Cool In T [°C]	Cool Out T [°C]	Delta T [°C]	T Ambiente [°C]	Flow rate (kg/s)	CSI [W/m2]	RSI [W/m2]
13-feb-18	(9-16)	48,8	53,7	5,0	15,2	0,1717	618,2	430,4

Table 4.9: data for February 13, 2018

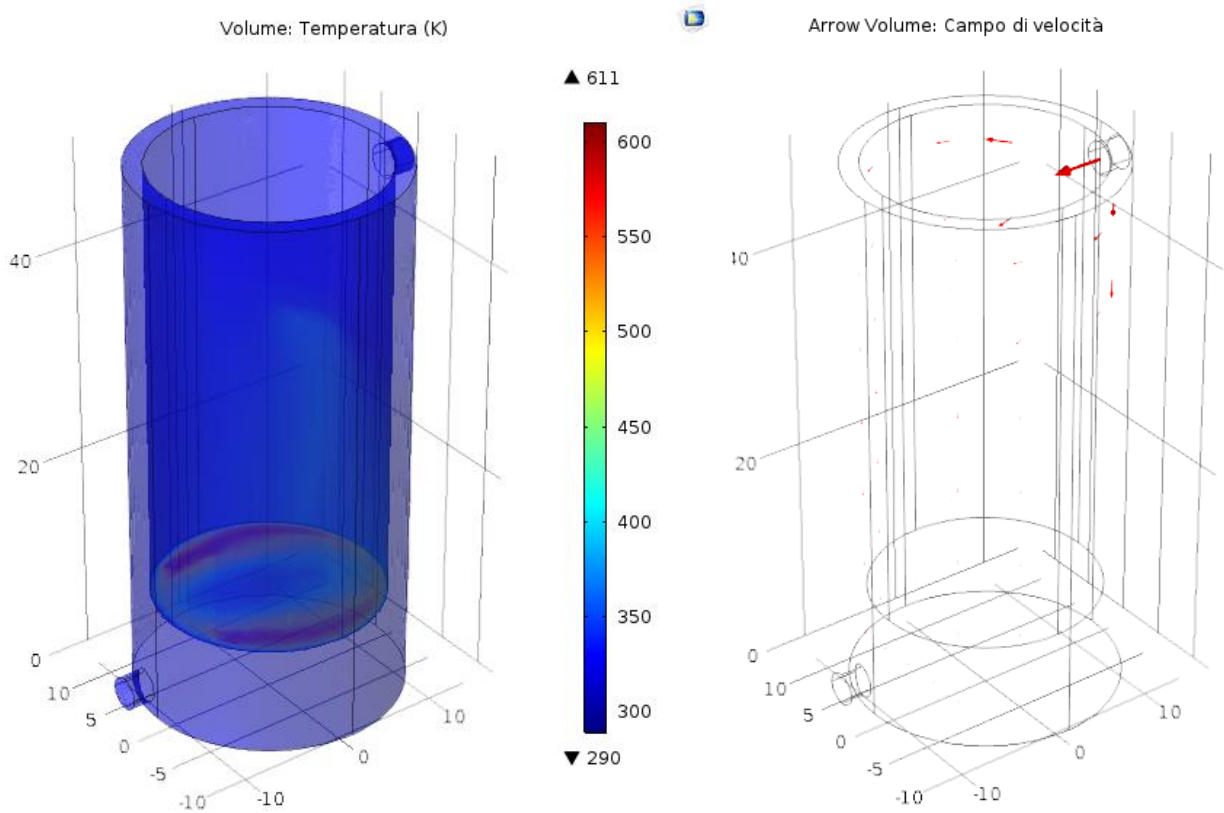


Figure 4.41: Temperature and velocity profile in the Turbocaldo system for February 13, 2018.

The outcome results are displayed in the following table:

	hours [h]	Cool In T [°C]	Experimental CO T [°C]	Experimental ΔT [°C]	Model CO T [°C]	Model ΔT [°C]	Error [%]
13-feb-18	(9-16)	48,8	53,7	5,0	53,9	5,1	3,2

Table 4.10: Results for February 13, 2018

Next day taken into analysis is February 14, 2018:

	hours [h]	Cool In T [°C]	Cool Out T [°C]	Delta T [°C]	T Ambiente [°C]	Flow rate (kg/s)	CSI [W/m ²]	RSI [W/m ²]
13-feb-18	(9-16)	48,8	53,7	5,0	15,2	0,1717	618,2	430,4

Table 4.11: data for February 14, 2018.

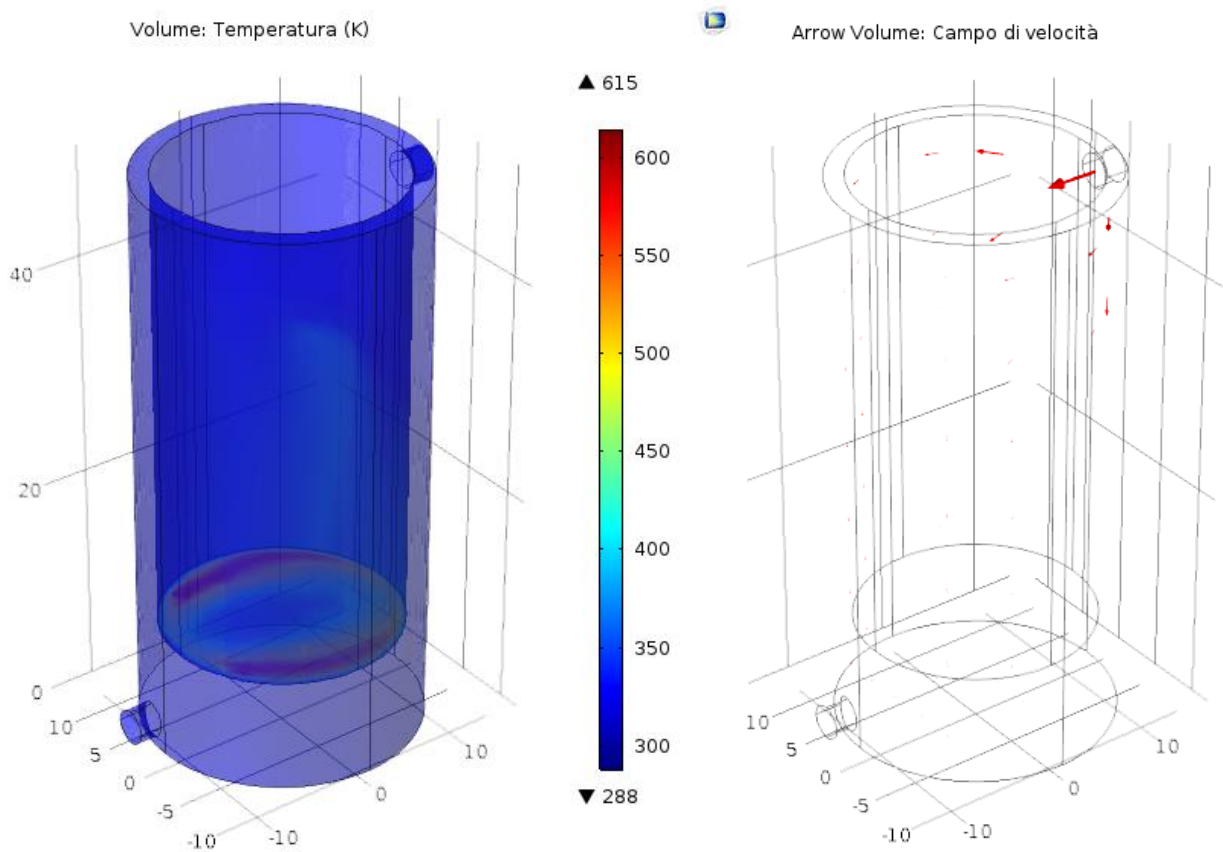


Figure 4.42: Temperature and velocity profile in the Turbocaldo system for February 14, 2018.

The outcome results are displayed in the following table

	hours [h]	Cool In T [°C]	Experimental CO T [°C]	Experimental ΔT [°C]	Model CO T [°C]	Model ΔT [°C]	Error [%]
14-feb-18	(9-16)	45,6	51,4	5,8	51,2	5,5	4,1

Table 4.12: Results for February 14, 2018.

In table 4.13 there is a recap of previous data analysis is shown, some approximations were made, in detail: optical efficiency was considered constant (89%), wind effect was considered constant and all parameters related to the transient weren't analyzed. Despite these approximation, as it may be seen the relative error for each day is less than 15%, which represents a good threshold for an experimental evaluation. Therefore, the model can be considered valid.

	hours [h]	Cool In T [°C]	Experimental CO T [°C]	Experimental ΔT [°C]	Model CO T [°C]	Model ΔT [°C]	Error [%]
07-mar-17	(8-16)	53,6	58,7	5,1	59,0	5,4	5,3
08-mar-17	(8-16)	51,5	57,0	5,5	57,7	6,2	12,5
26-nov-17	(9-13)	34,4	40,2	5,8	39,8	5,4	7,5
27-nov-17	(9-13)	40,0	45,3	5,3	44,6	4,6	12,2
13-feb-18	(9-16)	48,8	53,7	5,0	53,9	5,1	3,2
14-feb-18	(9-16)	45,6	51,4	5,8	51,2	5,5	4,1

Table 4.13: Recap of results for analyzed days.

Chapter 5

5 Coupling of the INNOVA parabolic solar concentrator dish with a desalination unit: feasibility study

Drinkable water is considered one of the primary goods for life, despite this according to the *United Nations Millennium Development Goals*, published in 2009, stated that 884 million people don't have improved drinking water; 84% of these live in rural or semirural areas [21]. In these areas desalination of the sea and brackish water has become necessary, even though there is usually lack in technologies and supplies, which make water purification very difficult, the abundance of sunlight may lead to a solution: the integration of solar power and desalination systems. [22]

Water filtration and distillation from sea water are known technologies, which need high energy quantities usually provided by fossil fuels [23]. The coupling of solar energy and desalination processes would be an important solution being environmentally friendly and because solar power is free. In order to make it possible both the time dependency of solar technologies and the heat demand of the desalination systems must be taken into account.

5.1 Membrane distillation

Desalination systems can be driven by solar energy in two ways:

- Solar energy is exploited to produce thermal energy required for the functioning of the desalination system,
- Solar energy can be exploited to produce electricity to feed components such as hydraulic pumps.

Membrane distillation is an Indirect collection system and it is the evaluated one for a possible coupling with the INNOVA system analyzed before.

The membrane distillation technology can be described as follows:

“Membrane distillation is a hybrid of thermal distillation and membrane processes best described as transmembrane evaporation. The driving force is a temperature difference between the feed water and permeate which results in a vapor pressure differential across a hydrophobic porous membrane (in contrast to pressure as driving force for RO and electrical potential as driving force for ED). Vapor evolved from the feed solution passes through the pores of the membrane and is collected on the other side. Since liquid does not penetrate the hydrophobic membrane, dissolved ions are completely rejected by the membrane.” [22]

As explained the driving force of this system is thermal energy used to create a temperature difference between a salty solution and a distillate, which are separated by a membrane. This temperature delta triggers an evaporation process due to different partial pressures, which depend on the amount of salt and on the temperature of the solution. [24]

It is now proposed a graphical representation of a membrane distillation setup.

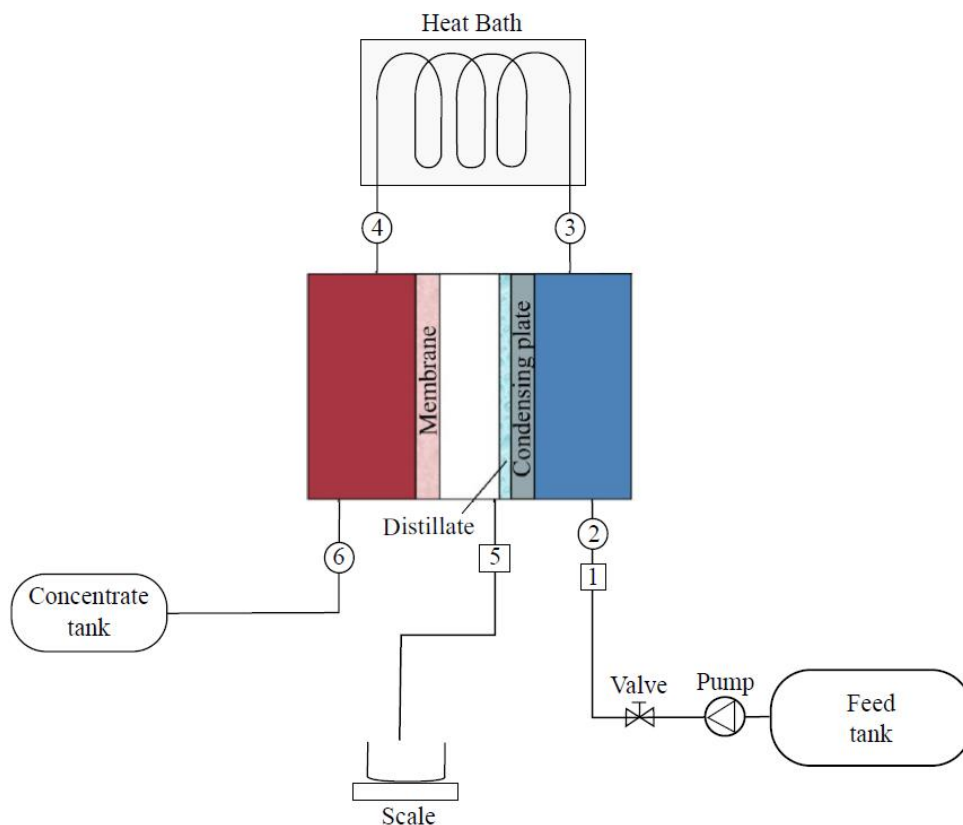


Figure 5.1: Schematic diagram of the membrane distillation setup. (1) feed conductivity sensor, (2) cold inlet thermocouple, (3) cold outlet thermocouple, (4) hot inlet thermocouple, (5) distillate conductivity meter, (6) hot outlet thermocouple. In our case the heat is supplied by the CSP system.

[A.J. Huges, T.S. O'Donovan, T. K. Mallick, *Experimental evaluation of a membrane distillation system for integration with concentrated photovoltaic/thermal (CPV/T) energy*, ICAER 2013]

As it may be seen in figure 5.1 between the membrane and the condensing plate there is an air gap, which leads to higher efficiencies [25], in other configurations the two are in direct contact.

5.2 Feasibility study

Few demonstration plants have been built exploiting solar energy to power up a thermal membrane distillation [26], some useful information can be exploited for this analysis. For instance, according to Hughes the process requires temperatures in the following range: 40°C – 85°C, and it can produce a maximum distillate flux of $3.4 \frac{l}{m^2h}$ [27]. Therefore, this temperature condition may be taken as necessary condition for the feasibility of the coupling.

5.2.1 Turin, Italy

The feasibility study is conducted on the INNOVA system installed in the Politecnico di Torino. As far as we can grasp from the PV GIS database, July results the most indicated month for the study, due to the highest values of external temperature and direct normal irradiance throughout the year. The extrapolated data for an 8-hour functioning (9:00-18:00) in Turin, in July, are shown in table 5.1.

	hours [h]	Cool In T [°C]	Outside Temp [°C]	Flow rate (kg/s)	CSI [W/m2]	RSI [W/m2]
Torino (July)	(9-18)	40	27	0,167	704,24	564,86

Table 5.1: Input data for the installation in Torino in June.

Exploiting the model previously built for the energetic characterization of the INNOVA system, the obtained results are:

	hours [h]	Cool in T [°C]	Cool out T [°C]	ΔT [°C]
Torino (July)	(9-18)	40	52,06	12,06

Table 5.2: Results for the installation in Torino in June.

Similar cool out temperatures can be found in the data records for June 2016, for few days, therefore all the following considerations are related to a specific situation and are not effective throughout the year.

As stated from the analysis the outlet temperature from the system is enough to sustain the desalination membrane process, therefore the coupling in July is feasible. To extend the working period to other less profitable months some precautions must be taken.

5.2.2 Aqaba, Jordan

Since the coupling between these two systems would be interesting for areas with much higher sunlight rate with respect to Turin, Italy, a further installation is analyzed.

Jordan is an Arab state in western Asia, it is mostly desert, but its western coasts lay on the Dead Sea; therefore, there is a great disposition of sunlight and sea water, and because of drought, a big need of fresh water. Aqaba, coastal city in Jordan, is the chosen spot for the installation analysis.

According to F. Banat and N. Jwaied paper on a real functioning plant assembled at Marine Science Station (MSS) of Aqaba the desalination process may be driven entirely from solar sources using seawater from the Red Sea directly as feed water. Assuming to keep the same membrane desalination system and changing the heat source with the INNOVA Turbocaldo, cool out temperatures of around 60-80°C are needed. [28]

To check the feasibility of this installation data related to the clear sky irradiance in Amman are taken from the PVG IS system (Photovoltaic Geographical Information System), as done before. The extrapolated data for an 8-hour functioning from 8:00 to 16:00 are shown in the following table:

	hours [h]	Cool In T [°C]	Outside Temp [°C]	Flow rate (kg/s)	CSI [W/m ²]	RSI [W/m ²]
Aqaba (Summer)	(8-16)	50	40	0,167	740,28	726,28

Table 5.3: Input data for Aqaba summer installation.

Exploiting the model built previously the results obtained are:

	hours [h]	Cool in T [°C]	Cool out T [°C]	ΔT [°C]
Aqaba (Summer)	(8-16)	50	67,66	17,66

Table 5.4: Results for Aqaba summer installation.

As stated before the cool out temperature of 60°C is easily reached throughout all summer, meaning that the coupling is feasible.

5.2.3 Diathermic oil

On the other hand, another approach could be considered in order to enlarge the installation sites. In detail diathermic oil allows the system to operate more efficiently also in milder climates. The mixture of water and glycol used guarantees good performances with low investment costs. To enhance the production, this fluid could be changed to improve performances.

A theoretical analysis is now conducted exploiting the previous model, using as heat transfer fluid a diathermic oil with these properties:

	Thermal Conductivity	Dynamic Viscosity	Density	Heat capacity at constant pressure
	k [W/m/K]	μ [Pa*s]	ρ [kg/m ³]	Cp [J/kg/K]
Diathermic oil	0,15	2,4	860	1842

Table 5.5: Diathermic oil properties.

Data related to climate such as irradiance and temperature are taken from the software PV GIS, using an average of values for May, June, July, August and September, to study functioning throughout all summer. The complete input data are shown in the following table:

	hours [h]	Cool In T [°C]	Outside Temp [°C]	Flow rate (kg/s)	CSI [W/m ²]	RSI [W/m ²]
Torino (Summer)	(9-18)	30	23,7	0,167	662,15	480,62

Table 5.6: Input data for summer evaluation in Torino.

Exploiting the model previously built for the energetic characterization of the INNOVA system, the obtained results are:

	hours [h]	Cool in T [°C]	Cool out T [°C]	ΔT [°C]
Torino (Summer)	(9-18)	30	112,93	82,93

Table 5.7: Results for summer evaluation in Torino.

These results express a very important increase in performance with respect to the use of the water-glycol mixture, therefore, with the use of a similar heat transfer fluid the power produced is enough to feed the desalination process, and, if wanted, some of the thermal power could also be stored in the highest operating days. To esteem the productivity of the system further analysis should be made.

It must be taken into account that changing the heat transfer fluid would also result into a deep evaluation of pipes and circulating system, in order to avoid malfunctioning due to different density, expansion coefficient and other thermodynamic parameters. In addition to that the investment cost and the operating and maintenance costs must be taken into account, since they would be higher with respect to the water-glycol mixture.

In conclusion the coupling between these two systems could be feasible and the performances would depend heavily on the site of installation and on the chosen heat transfer fluid.

Conclusions

In recent years the drastic worsening of climatic and environmental conditions, correlated with the constant increase in the production of greenhouse gases, has led the international scientific community to raise awareness on the topic of renewable energy sources, whose contribution is essential for the fulfillment of the conditions promulgated with the Paris Agreement. The replacement of fossil fuels requires, in the field of energy production, the optimization of conversion, transport and storage systems, as well as important initial investments.

In this work a solar concentration device was treated for the production of thermal energy (<10kW) and its energetic characterization, in terms of fundamental parameters such as efficiency and thermal power, was carried out. The system exploits a reflecting surface of parabolic shape to concentrate, with high precision, the incident direct solar radiation inside the cavity of a compact metal receiver placed near the focal point. The configuration guarantees a high efficiency of absorption and reduced thermal dispersion, due to the reduced dispersing surface in contact with the external environment. The absorber acts as a heat exchanger with the circuit containing the heat transfer fluid, which carries heat into tanks in order to be stored. The analysis shows that the conversion efficiency, calculated as the ratio between the thermal power absorbed by the liquid and the incident solar radiation, reaches good values (60-70%), which are often better than competitors on the market, such as vacuum tubes and flat plate collectors.

In perspective, CSP could become a much more interesting technology if coupled with innovative materials in order to highly enhance its performance. For instance, in order to improve the solar cavity receiver, nanofluids could be implemented, which have larger optical absorption coefficients [29]. On the other hand, the improvements could be related to the secondary circuit, perhaps by implementing heat storage systems based on adsorption processes, such as zeolites [30]. Improvements like these ones could make the CSP devices suitable both for domestic applications, such as domestic hot water supply and air conditioning systems, and for industrial uses, such as seawater desalination.

Seawater solar desalination is a promising method to produce fresh water in areas where sunshine is abundant and there is a major lack of water. Developing sustainable technologies is necessary for reducing the environmental impact of energy systems in the world. In this work a brief overview on the coupling of the CSP technology with a desalination system has been studied. Results stated that due to the necessary high operating temperature, this coupling could reach interesting results if installed in areas where sunshine is abundant and constant throughout the year, or with the substitution of the heat transfer fluid with a more performing one. On the other hand, with a clever selection and assembly of common materials,

interesting results can be reached too. In perspective, with a desirable reduction of the investment costs and a further development of the technology, this system may be seen as an interesting project to solve a major problem.

Reference List

- [1] http://unfccc.int/essential_background/convention/items/6036.php
- [2] http://unfccc.int/paris_agreement/items/9485.php
- [3] https://ec.europa.eu/clima/policies/strategies/2020_en
- [4] Eisberg-Resnick, *Quantum Physics - Chapter 1*
- [5] Kuo-Nan Liou, *An Introduction to Atmospheric Radiation – Chapter 3*
- [6] John A. Duffie, and William A. Beckman, *Solar Engineering of Thermal Processes*, Wiley, 2013
- [7] Kalogirou SA. *Solar energy engineering: processes and systems*. Academic Press; 2009
- [8] D. Barlev, R. Vidu, P. Stroeve, *Innovation in concentrated solar power, Solar Energy Materials and Solar Cells*, 2011.
- [9] A.W. Badar, R. Buchholz, F. Ziegler, *Experimental and theoretical evaluation of the overall heat loss coefficient of vacuum tubes of a solar collector*, 2011.
- [10] *Measurement of Domestic Hot Water Consumption in Dwellings*, Energy monitoring Company,
- [11] Ugo Pelay, Lingai Luo, Yilin Fan, Driss Stitou, Mark Rood, *Thermal energy storage systems for concentrated solar power plants*, 2017
- [12] Y. T. Shah, *Thermal Energy: Sources, Recovery, and Applications*, Crc Press, Taylor & Francis Group, 2018.
- [13] Robert Pitz Paal, *Future Energy - Improved, Sustainable and Clean Options for Our Planet*, 2008.
- [14] K. Lovegrove, W. Stein, *Concentrating Solar Power Technology: Principles, Developments and Applications*, Elsevier Science & Technology, 2012.
- [15] W.B. Stine and R.W. Harrigan, *Solar Energy Systems Design*, 1986, <http://www.powerfromthesun.net/>
- [16] A. Giovannelli, *State of the Art on Small-Scale Concentrated Solar Power Plants*, 2015
- [17] S. Shanmugama, M. Eswaramoorthyb, and A. R. Veerappana, *Mathematical Modeling of Thermoelectric Generator Driven by Solar Parabolic Dish Collector*, 2010;
- [18] TRINUM, *Technical Manual for Installation and Use*, 2014;
- [19] Tigi, *Solar collectors efficiency*, 2016.
- [20] G.J. Prinsloo, R.T. Dobson, *Solar Tracking: High precision solar position algorithms, programs, software and source code for computing the solar vector, solar coordinates & sun angles in Microprocessor, PLC, Arduino, PIC and PC-based sun tracking devices or dynamic sun following hardware*, 2015;

- [21] Department of Economic and Social Affairs, *The Millennium Development Goals Report*, United Nations, New York, 2009.
- [22] F. Banat, N. Jwaied, *Desalination by a “compact SMADES” autonomous solar powered membrane distillation unit*, 2006
- [23] S. Miller, H. Shemer, R. Semiat, *Energy and environmental issues in desalination*, 2015.
- [24] E. Chiavazzo, M. Morciano, F. Viglino, M. Fasano, P. Asinari, *Passive high-yield seawater desalination at below one sun by modular and low-cost distillation*, 2017.
- [25] M. Morciano, M. Fasano, U. Salomov, L. Ventola, E. Chiavazzo, P. Asinari, *Efficient steam generation by inexpensive narrow gap evaporation device for solar applications*, 2017.
- [26] J. Koschikowski, M. Wiegghaus, M. Rommel, *Experimental investigations on solar driven stand-alone membrane distillation systems for remote areas*, 2009.
- [27] A.J. Huges, T.S. O'Donovan, T. K. Mallick, *Experimental evaluation of a membrane distillation system for integration with concentrated photovoltaic/thermal (CPV/T) energy*, ICAER 2013.
- [28] F. Banat, N. Jwaied, M. Rommel, J. Koschikowski, M. Wiegghaus, *Performance evaluation of the “large SMADES” autonomous desalination solar-driven membrane distillation plant in Aqaba, Jordan*, 2006.
- [29] A Moradi, E Sani, M Simonetti, F. Francini, E. Chiavazzo, P. Asinari, *Carbon-nanohorn based nanofluids for a direct absorption solar collector for civil applications*, Renewable and Sustainable Energy Reviews, 2016.
- [30] M. Fasano, D. Borri, E. Chiavazzo, P. Asinari, *Protocols for atomistic modelling of water uptake into zeolite crystals for thermal storage and other applications*, Applied Thermal Engineering, 2016.

Acknowledgements

This thesis represents for me the end of the most important formative experience of my life, thanks to all those who were part of it, directly or indirectly, without which this work would not have been possible.

I would like to thank prof. Asinari, supervisor of this thesis, for the help, the availability and the precision shown during the drafting period. A big thank you also goes to Matteo, who followed me step by step and deeply helped me in the preparation and conclusion of this project.

Heartfelt thanks go to my family who, with untiring support, has allowed me to complete my training period. I would like to thank my parents who represent two models to follow since my childhood and who I will never thank enough. I really hope I have made them proud. Big thanks to my brother Dado, who has often demonstrated support and esteem, representing an incentive to achieve this goal.

Thank you, Lorenzo, Claudia, Sara, Stefano, Franc, Silvia and all those with whom I shared the joys and sorrows of the university career and that allowed me to face the reality of the Polytechnic with the necessary grit and awareness to achieve many satisfactions.

Deepest thanks to all my friends who accompanied me on this journey outside the walls of the Polytechnic, which helped me to unite the university efforts with the lightheartedness and joy that are fundamental to me. A big thank you to Angelo, Alessandro, Antonio, Edoardo, Edoardo, Fabio, Giovanni, Jacopo and all the others.

Final thanks go to my girlfriend who is for me a point of reference, she was next to me, she supported me and gave me serenity in the most difficult moments of my university career. Thank you, Camilla.